Mineralogy and Petrology (2008) 92: 361–391
DOI 10.1007/s00710-007-0198-0
Printed in The Netherlands

Mineralogy and Petrology

Geochemistry and Sr-Nd isotope systematics of metabasites in the Tunchang area, Hainan Island, South China: implications for petrogenesis and tectonic setting

D. Xu[1,2,*], **B. Xia**[1], **N. Bakun-Czubarow**[2], **R. Bachlinski**[2], **P. Li**[1], **G. Chen**[1], and **T. Chen**[1]

[1] Chinese Academy of Sciences, Guangzhou Institute of Geochemistry, Guangzhou, People's Republic of China
[2] Polish Academy of Sciences, Institute of Geological Sciences, Warszawa, Poland

Received September 17, 2005; revised version accepted June 20, 2007
Published online October 18, 2007;
Editorial handling: J. Foden and J. Raith

Summary

The metabasites in Tunchang area, East-central Hainan Island, South China generally display strongly LREE-depleted patterns, extremely low HFSE concentrations and relatively high LILE contents; a few boninite-like samples have a concave-up, slightly LREE-enriched pattern. The low but variable Ti/V ratios between 6 and 20, and the high mg-numbers and Cr, Co, Ni contents, are indicative of plume-influenced intra-oceanic arc magmas. It accord with this model are moderately high $\varepsilon_{Nd}(t)$ values ranging from +2.16 to +6.75, and $^{87}Sr/^{86}Sr_i$ values ranging from 0.70239 to 0.70824. These geochemical features imply that the protoliths for the Tunchang area metabasites are relics of an intra-oceanic island arc and the parental melts of these rocks were generated from a depleted, primitive mantle arc source rather than from a N-MORB source in a supra-subduction zone-like setting. The minor geochemical differences between the two identified groups of metabasites are due to a combined result of the variable degree of partial melting and the crystal fractionation of clinoproxene ± olivine ± plagioclase.

The Tunchang area metabasites are distinctive in geochemical and isotopic compositions, and likely also in age from the Bangxi area metabasites in the northwestern part of Hainan Island. We assume that the NE–SW trending Baisha Fault Zone likely marks an early suture zone due to the collision of an Early Paleozoic intra-oceanic arc with the

* Present address: Chinese Academy of Sciences, Guangzhou Institute of Geochemistry, Guangzhou, Guangdong Province 510640, People's Republic of China

South China continent. In contrast, the Bangxi area metabasites more likely are formed in an extensional back-arc basin due to subduction of the Paleo-Tethys beneath the South China continental margin during the Late Paleozoic.

Introduction

Many geoscientists have recognized that ophiolites might have been derived from different mantle provenances and formed in a variety of tectonic settings (e.g., spreading mid-ocean ridges, back-arc spreading centers, supra-subduction zones) (*Yumul*, 2003 and references therein). Especially, supra-subduction zone-related tectonic models (SSZ) provide alternative models for the genetic interpretation of many ophiolites (e.g., *Robertson*, 2002). Ophiolites with SSZ-type geochemical signature, such as the Troodos ophiolite from Cyprus (for a review see *Coogan* et al., 2003), are distinguished from normal MORBs in major- and trace elements as well as in isotopes.

Paleozoic metabasites widely crop out on Hainan Island, South China (Fig. 1). Their origin and geotectonic significance have been controversial among Chinese geoscientists. The geochemical and isotopic data seem to support an interpretation of these rocks as relics of fragmented oceanic crust of the eastern part of the Paleo-Tethys (*Li* et al., 2002). However, the results of previous studies are not compatible with such an interpretation and the previously geological, petrographic and geochemical data are in favor of an intercontinental rift related to lithosphere thinning

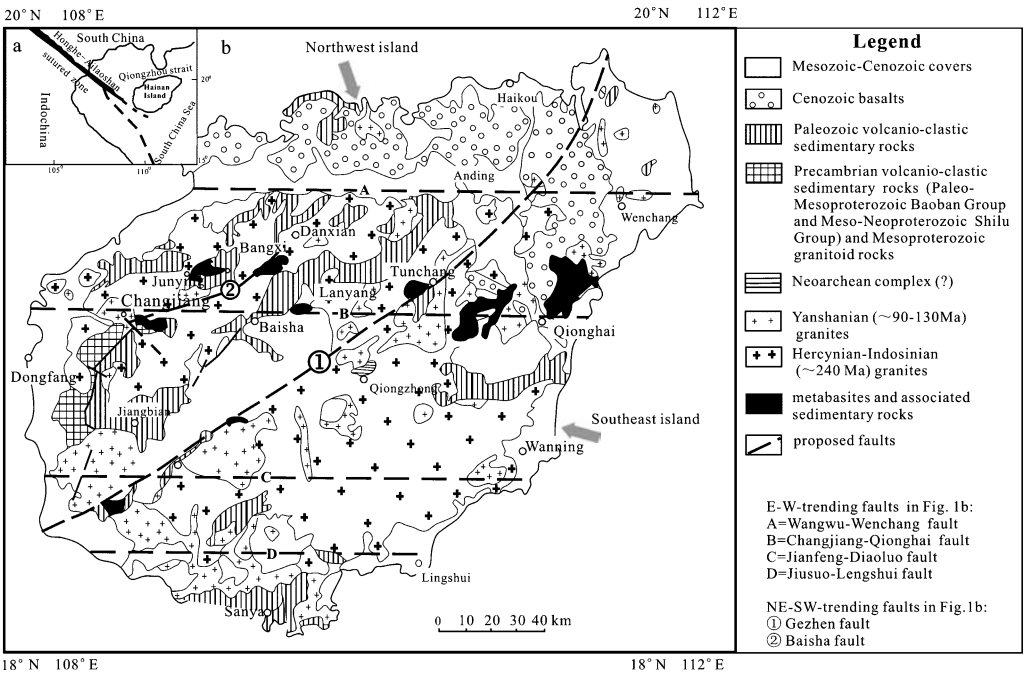

Fig. 1. Simplified geological map of Hainan Island showing the main tectono-stratigraphic and tectono-magmatic units. The tectono-stratigraphic division of Hainan Island into the Southeast and the Northwest Islands is according to *Metcalfe* et al. (1993)

(*Xia* et al., 1991; *Fang* et al., 1992). Hence, further documentation of petrogenetic scenario and tectonic settings responsible for these rocks is required. Based on new petrographical, bulk rock geochemical and Sr-Nd isotopic data of the metabasites in Tunchang area, East-central Hainan Island, this study attempts to determine their possible provenance and genesis, and their representative tectonomagmatic events.

Field geology and petrography

Hainan Island, separated from the Cathaysian Block of South China by Qiongzhou Channel (Fig. 1a), is a continental-type island. Abundant metabasites, occurring as small, isolated lensoid and/or stratiform bodies within the Paleozoic volcanioclastic sedimentary sequences of marine to terrestrial facies origin, are present mainly along both sides of the E–W trending Changjiang-Qionghai and the NE–SW trending Baisha Fault Zones on this Island (Fig. 1b).

The metabasites in Tunchang area, in the East-central Island, are situated between Yashiyuan and Xichangyuan (longitude and latitude 109°57′22″ to 109°58′15″ and 19°25′30″ to 19°26′15″, respectively Fig. 2). Our field investigations indicate that this wedge-shaped body has a NE-trending axis and is about 3.0 km long and about 0.6 km wide. Its main foliation and associated (mineral) lineation are NNE-NNW trending and are roughly dipping E at an angle of about 50–70° (Fig. 2a). The Carboniferous (?) host rocks comprise of a set of huge, thick,

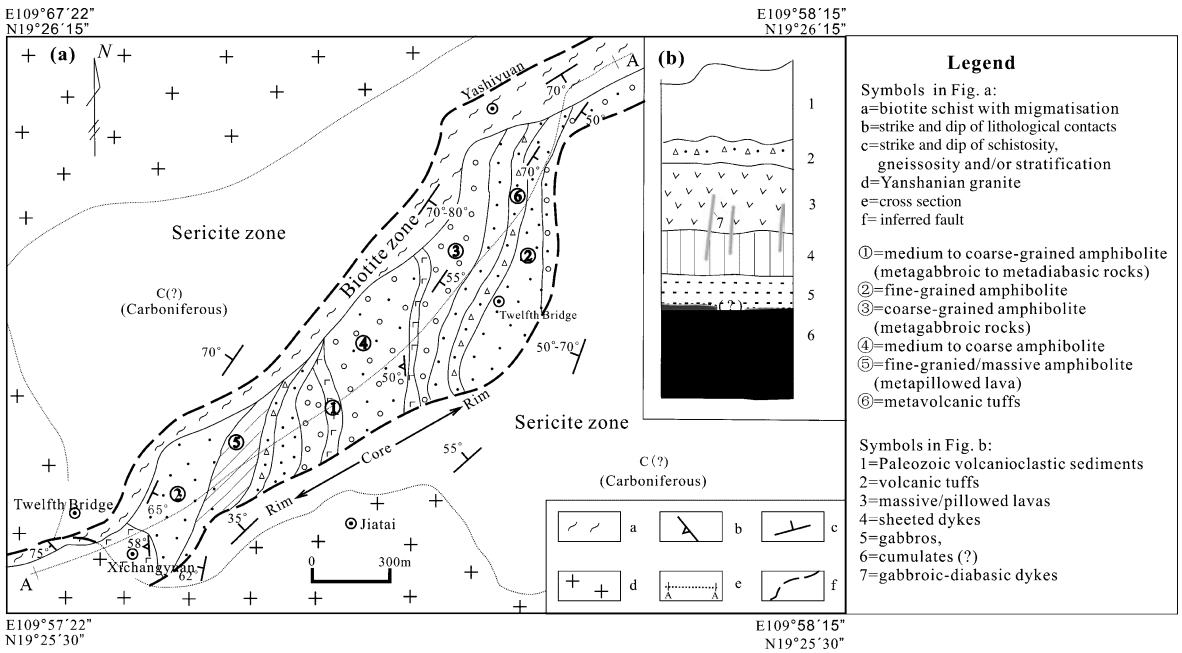

Fig. 2. (**a**) Geological map showing the Tunchang area metabasites in the East-central Hainan Island. (**b**) Schematic cross section through the possible ophiolitic unit. The metabasites are generally fine-grained near the margins and become coarse-grained towards the cores; they are crosscut by diabasic-gabbroic dykes indicating an incomplete, dismembered ophiolitic suite

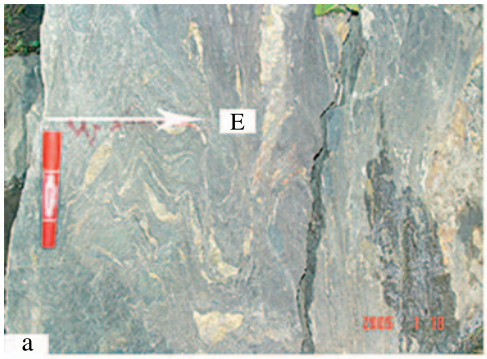
E
a

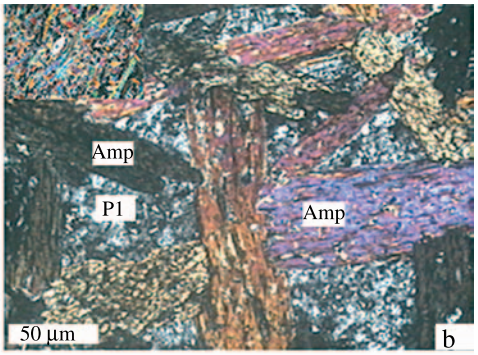
Amp
P1
Amp
50 μm
b


c

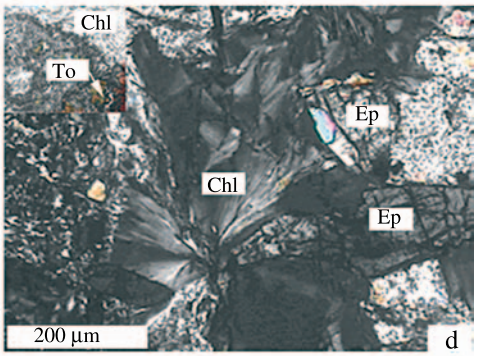
Chl
To
Ep
Chl
Ep
200 μm
d

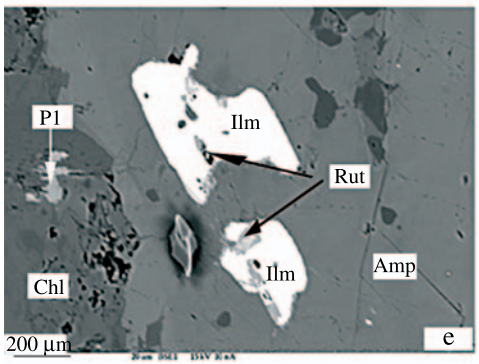
P1
Ilm
Rut
Ilm
Amp
Chl
200 μm
e

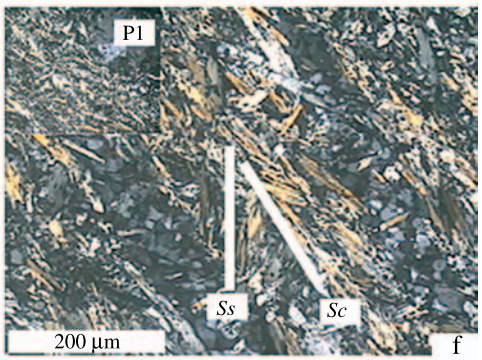
P1
Ss
Sc
200 μm
f

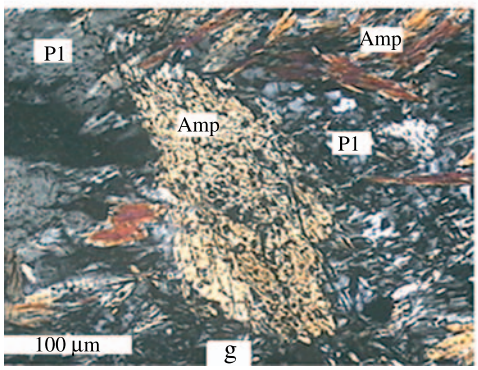
P1
Amp
Amp
P1
100 μm
g

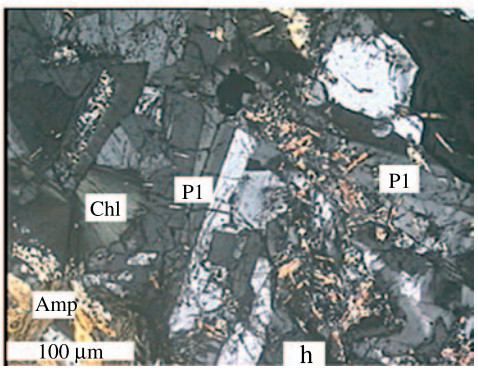
P1
P1
Chl
Amp
100 μm
h

low grade argillaceous, arenaceous and silicious sediments of middle-deep marine facies origin. Two metamorphic zones, i.e. a sericite and the biotite zone, have been identified in the studied area (Fig. 2a), based on the first appearance of the index mineral biotite. The biotite zone only occurs locally in the western part of the metabasite body and has a width of about 50–200 m. Up to meter-scale tight to isoclinal folds and possible migmatisation are also observed in this zone (Fig. 3a). The identical strike and dip to the metabasite body suggest occurrence of this zone as an interlayer with the latter. The sericite zone occurs extensively in the studied area and generally exhibits NE-trending planar fabrics, which are roughly dipping W at an angle of 35–70°. A fault contact, respectively in the northwest and the southeast, probably marks the boundary between the sericite zone and the metabasite body (Fig. 2a).

The rock assemblages of the Tunchang area metabasites comprise coarse-grained, medium to fine-grained and massive amphibolites, and appear to be cross-cut by medium to coarse-grained amphibolites (Fig. 2a). The coarse-grained amphibolites are dark and dark-green in color, and contain radiating clusters of green, prismatic amphibole with a length of 0.5–3 cm, and milky, porphyritic plagioclases with a size of about 0.5–1 cm. These amphibolites often show after a homogeneous, poikilitic texture and pseudomorphis of amphiboles pyroxenes (Fig. 3b); thus their protoliths are proposed to have been gabbroic rocks. The medium to fine-grained, massive/or fine-grained but more foliated texture amphibolites of green-grey to green color are equigranular and have the same mineral assemblage as their coarse-grained equivalents. Relics of pillowed structures have been well preserved in these rocks (Fig. 3c). Rare metavolcanic tuff covers the underlying meta-pillow lava.

The Tunchang area metabasites show variable degrees of metamorphism, alteration and shear deformation. Magmatic minerals, such as pyroxene, olivine and/or hornblende, are no longer preserved in these rocks. Abundant chlorites with a color ranging from colorless to green occur as fibrous-radiating chlorite aggregates (Fig. 3d) and/or as chlorite-bearing veinlets. Ubiquitous plagioclase is altered to more sodic plagioclase and prehnite. Ilmenite is very abundant and appears as xenomorphic or even skeletal grains, whereas minor rutile occurs in ilmenite (Fig. 3e). Minor muscovite and tourmaline occur as secondary minerals. Fine-grained rocks have a perfect nematoblastic texture defined by oriented amphibole and/or plagioclase along the schistosity (Fig. 3f). The amphibole from the coarse-grained samples does not show such a well-expressed mineral orientation, but commonly

Fig. 3. Field photographs and thin-section photomicrographs for Tunchang area metabasites and their associated host rocks in the East-central Hainan Island. Pen and hammer in field photographs (**a**) and (**c**) for scale. **e** BSE image, all others are photomicrographs taken with crossed nicols. (**a**) biotite-bearing schist with migmitisation and isoclinal folding, (**b**) poikilitic texture shown by amphiboles, sample TC008-1 (upper-left inset for sample TC006-1), (**c**) metapillowed structure, (**d**) fibrous, radiating chlorite aggregate, sample YSY-06 (upper-left inset in plane-polarized light), (**e**) rutile inclusion within ilmenite, sample TC001-1, (**f**) *S-C* fabrics, sample 12B-08, (**g**) fish-like amphibole, sample YSY-01 and (**h**) metagabbroic-metadiabasic texture, sample YSY04-2. *Amp* amphibole; *Pl* plagioclase; *Chl* chlorite; *Ep* epidote; *To* tourmaline; *Ilm* ilmenite and *Rut* rutile

Table 1. *Bulk-rock major and trace elements analyses for the Tunchang area metabasites in the East-central Hainan Island, South China*

Group	Group 1														
Rock type	Basalt	Basalt	Basalt	Basalt	Basalt	Basalt	Basalt	Basalt	Gabbro	Basalt	Gabbro	Gabbro	Gabbro	Gabbro	Gabbro
Grain size	fine	fine	fine	fine	fine	fine-medium	coarse	fine-medium	coarse	fine	fine-medium	coarse	medium-coarse	medium-coarse	medium-coarse
Samples	YSY-03	YSY-02	12B-07	12B-08	12B-09	YSY04-1	YSY-01	YSY04-2	TC001	TC004	YSY-06	YSY05-1	YSY05-2	TC002	TC003
SiO_2	51.81	57.86	55.00	53.40	56.24	53.18	52.20	54.40	56.79	57.14	52.52	51.37	51.50	57.03	55.00
TiO_2	1.24	1.23	1.61	1.59	1.82	0.99	1.38	0.90	0.71	0.56	1.13	0.87	0.88	0.38	0.39
Al_2O_3	16.96	14.32	15.10	15.86	14.57	17.85	15.19	15.72	14.76	13.82	14.46	13.14	14.35	16.06	13.99
MgO	7.26	6.09	5.04	6.00	5.46	7.39	8.82	8.57	9.91	8.31	13.15	15.56	15.18	7.07	10.10
FeO*	6.61	5.54	7.96	8.19	8.68	6.64	7.66	6.84	4.36	5.16	6.80	7.95	6.71	5.12	4.63
MnO	0.10	0.11	0.12	0.18	0.15	0.11	0.14	0.18	0.18	0.17	0.08	0.03	0.11	0.15	0.16
CaO	14.42	13.03	12.83	12.24	10.66	11.24	12.76	11.17	9.11	9.27	10.10	9.73	9.73	9.52	9.02
Na_2O	1.02	1.31	1.83	2.11	2.00	1.76	1.44	1.74	2.94	3.27	0.97	0.71	0.93	1.91	3.06
K_2O	0.14	0.13	0.12	0.10	0.11	0.56	0.08	0.18	0.21	0.20	0.25	0.36	0.33	0.23	0.27
P_2O_5	0.43	0.39	0.41	0.32	0.32	0.29	0.32	0.31	n.a	n.a	0.53	0.28	0.29	n.a	n.a
LOT	3.75	3.49	2.37	3.50	2.35	3.96	4.09	2.90	0.78	1.69	3.90	3.50	3.96	2.12	2.87
CO_2	1.70	1.10	2.00	1.90	1.99	1.40	1.20	1.10	n.a.	n.a.	0.90	1.05	1.00	n.a.	n.a.
Total	99.48	99.60	99.62	99.50	99.46	99.31	99.54	99.37	99.74	99.58	99.47	99.43	99.41	99.58	99.49
$Mg^{\#}$	69	69	56	59	55	69	70	71	82	76	79	79	82	73	81
Mn	2270.4	1673.2	1733.7	1938	2218.8	1490.4	2128.5	1785.0	n.a.	n.a.	1832.7	2013.1	2024.7	n.a.	n.a.
Co	135.5	104.1	86.3	77.7	104.9	96.9	110.1	90.9	70.0	49.0	101.5	117.6	106.6	83.0	70.0
Cr	2319.6	1621.6	664.9	724.1	710.2	1502.1	1317.6	2011.5	676.0	631.0	1909.6	3055.1	2822.3	1114.0	865.0
Ni	398.7	278.0	110.7	105.0	216.2	262.2	297.9	325.7	165.0	240.0	312.0	514.2	470.5	315.0	303.0
V	415.8	356	502.5	506.8	523.8	345.8	422	319.3	374	306	316.6	349.8	365.7	297	293
Zr	9.867	10.74	12.4	14.98	23.72	10.24	19.77	10.45	n.a.	n.a.	8.085	14.16	10.1	n.a.	n.a.
Cu	102.4	86.68	130.7	127.1	128.2	69.82	113.7	34.51	167	61	40.48	30.26	35.9	28	83
Zn	72.94	46.74	47.11	1069.6	1017.6	2465.3	65.46	54.3	n.a.	n.a.	73.76	81.17	91.48	n.a.	n.a.
Ga	15.8	11.84	14.47	14.79	14.6	11.94	13.02	10.9	n.a.	n.a.	10.93	9.587	9.702	n.a.	n.a.
Ge	2.072	2.165	2.32	2.069	2.006	2.048	1.97	2.059	n.a.	n.a.	2.261	2.555	2.457	n.a.	n.a.
Cs	3.72	0.611	0.105	0.109	0.277	21.68	0.317	1.027	n.a.	n.a.	3.932	0.873	1.54	n.a.	n.a.

(*continued*)

Table 1 (*continued*)

Group	Group 1														
Rock type	Basalt	Basalt	Basalt	Basalt	Basalt	Basalt	Basalt	Basalt	Gabbro	Basalt	Gabbro	Gabbro	Gabbro	Gabbro	Gabbro
Grain size	fine	fine	fine	fine	fine	fine-medium	coarse	fine-medium	coarse	fine	fine-medium	coarse	medium-coarse	medium-coarse	medium-coarse
Samples	YSY-03	YSY-02	12B-07	12B-08	12B-09	YSY04-1	YSY-01	YSY04-2	TC001	TC004	YSY-06	YSY05-1	YSY05-2	TC002	TC003
Ba	51.42	180.5	23.74	69.51	37.06	221.6	49.68	39.91	67	201	41.75	226.9	201.4	117	197
Y	18.15	15.04	25.41	26.04	27.9	14.36	21.85	14.73	n.a.	n.a.	13.85	11.35	11.38	n.a.	n.a.
La	1.062	0.751	1.059	1.165	1.502	0.611	0.913	0.515	n.a.	n.a.	1.114	0.516	0.768	n.a.	n.a.
Ce	3.267	2.48	3.465	3.745	4.591	2.074	2.915	1.706	n.a.	n.a.	3.202	1.882	2.273	n.a.	n.a.
Pr	0.624	0.497	0.702	0.742	0.888	0.442	0.594	0.367	n.a.	n.a.	0.558	0.412	0.429	n.a.	n.a.
Nd	3.547	2.997	4.216	4.497	5.243	2.7	3.647	2.185	n.a.	n.a.	2.974	2.316	2.481	n.a.	n.a.
Sm	1.386	1.149	1.738	1.876	2.092	1.08	1.534	0.892	n.a.	n.a.	1.054	0.938	0.962	n.a.	n.a.
Eu	0.644	0.526	0.788	0.808	0.788	0.348	0.679	0.398	n.a.	n.a.	0.474	0.617	0.543	n.a.	n.a.
Gd	2.498	2.074	3.154	3.34	3.754	1.98	2.759	1.737	n.a.	n.a.	1.887	1.689	1.759	n.a.	n.a.
Tb	0.441	0.371	0.577	0.606	0.693	0.366	0.508	0.328	n.a.	n.a.	0.339	0.329	0.328	n.a.	n.a.
Dy	2.992	2.57	3.992	4.178	4.594	2.522	3.547	2.327	n.a.	n.a.	2.249	2.18	2.254	n.a.	n.a.
Ho	0.652	0.564	0.894	0.927	0.997	0.563	0.782	0.514	n.a.	n.a.	0.502	0.496	0.499	n.a.	n.a.
Er	1.883	1.665	2.689	2.733	3.025	1.666	2.368	1.561	n.a.	n.a.	1.499	1.409	1.532	n.a.	n.a.
Tm	0.308	0.261	0.435	0.439	0.47	0.259	0.372	0.252	n.a.	n.a.	0.232	0.228	0.234	n.a.	n.a.
Yb	2.035	1.724	2.852	2.916	3.115	1.705	2.467	1.638	n.a.	n.a.	1.505	1.503	1.542	n.a.	n.a.
Lu	0.327	0.289	0.455	0.47	0.521	0.269	0.403	0.263	n.a.	n.a.	0.241	0.248	0.255	n.a.	n.a.
Rb	5.93	2.294	0.581	0.927	0.81	24.72	2.36	9.139	20	15	11.08	12.62	14.53	27	34
Sr	246.6	173	64.92	165.1	126.2	478.8	56.2	320.4	27	174	267.2	40.96	37.51	37	145
Hf	0.411	0.401	0.498	0.562	0.785	0.381	0.735	0.387	n.a.	n.a.	0.309	0.404	0.354	n.a.	n.a.
Sc	49.03	42.87	50.28	48.83	50.16	42.65	44.03	41.76	n.a.	n.a.	38.59	33.19	31.05	n.a.	n.a.
Nb	0.607	0.367	0.797	0.886	1.331	0.317	0.671	0.312	n.a.	n.a.	0.525	0.392	0.627	n.a.	n.a.
Ta	0.052	0.033	0.061	0.067	0.101	0.026	0.05	0.024	n.a.	n.a.	0.04	0.029	0.042	n.a.	n.a.
Pb	85.77	1.313	0.869	1.379	2.582	5.341	2.464	4.784	63	53	5.159	3.469	5.546	52	78
Th	0.12	0.039	0.062	0.149	0.1	0.035	0.05	0.036	n.a.	n.a.	0.06	0.04	0.179	n.a.	n.a.
U	0.066	0.113	0.024	0.035	0.037	0.034	0.015	0.075	n.a.	n.a.	0.044	0.017	0.038	n.a.	n.a.
Ti	5967.2	4996.1	7857.3	7956.2	9385.9	4365.0	6559.5	4154.3	4261.1	3341.3	4489.9	2212.2	2100.9	2250.9	2346.8

(*continued*)

Table 1 (*continued*)

Group	Group 1	Group 2												
Rock type	Grabbro	Basalt	Gabbro	Gabbro	Gabbro	Gabbro	Gabbro	Gabbro	Gabbro	Gabbro	Gabbro	Gabbro	Gabbro	Doleritic rock
Grain size	medium-coarse	fine	coarse	coarse	coarse	coarse	coarse	coarse	coarse	coarse	coarse	coarse	coarse	medium-fine
Samples	TC006	TC004-1	TC007-1	TC008-1	TC001-1	CX-1	CX-2	CX-3	CX-4	CX-5	CX-6	D91001	D91002	TC006-1
SiO_2	55.51	47.95	55.01	54.57	51.18	49.97	47.96	47.40	50.92	44.78	45.84	48.82	47.85	52.65
TiO_2	0.47	0.57	0.67	0.71	0.57	0.56	0.62	0.41	0.39	0.50	0.47	0.80	0.74	0.46
Al_2O_3	17.12	16.28	11.98	12.13	15.07	12.24	14.62	13.43	12.63	15.41	15.21	16.21	15.83	12.46
MgO	6.38	12.52	9.55	9.31	11.09	13.18	12.32	11.64	10.71	13.78	11.94	11.30	7.95	13.03
FeO*	5.24	9.05	8.81	8.62	7.59	9.80	10.06	9.79	7.97	11.00	10.59	9.25	9.98	7.47
MnO	0.13	0.18	0.20	0.19	0.18	0.15	0.16	0.17	0.15	0.15	0.14	0.13	0.10	0.16
CaO	9.94	12.09	10.77	11.39	12.30	12.31	12.26	15.31	14.77	12.62	14.00	10.87	14.52	11.65
Na_2O	2.87	1.21	2.78	2.80	1.61	1.74	1.31	1.39	2.12	0.98	1.17	2.04	2.30	1.75
K_2O	0.10	0.09	0.20	0.23	0.37	0.19	0.82	0.63	0.50	0.93	0.79	0.50	0.49	0.17
P_2O_5	n.a	0.04	0.04	0.04	0.04	0.05	0.05	0.02	0.02	0.03	0.03	0.08	0.25	0.22
LOT	1.71	3.28	2.38	2.55	2.43	1.52	2.16	3.02	2.52	3.29	2.54	n.a.	n.a.	2.57
CO_2	n.a.	0.08	0.18	0.49	0.19	n.a.	n.a.	n.a.	n.a.	n.a.	n.a.	n.a.	n.a.	0.06
Total	99.47	99.37	99.37	99.37	99.37	101.71	102.34	103.21	102.70	103.47	102.72	100.0	100.0	99.37
$Mg^{\#}$	71	73	68	68	74	73	71	70	73	71	69	71	61	78
Co	80	48	32	37	38	59.90	59.00	58.00	46.50	60.50	55.50	n.a.	n.a.	47
Cr	527	1027	536	543	717	887.00	881.00	1006.00	769.00	1192.00	1091.00	n.a.	n.a.	1013
Ni	245	270	160	186	174	382.00	337.00	280.00	211.00	275.00	322.00	n.a.	n.a.	402
V	295	192	234	221	179	197.00	216.00	181.00	180.00	260.00	198.00	n.a.	n.a.	143
Zr	n.a.	27	31	31	27	34.00	36.50	24.30	20.10	22.60	22.90	n.a.	n.a.	30
Cu	163	67	17	24	25	48.9	29.3	56.8	14.6	80	94.8	n.a.	n.a.	22
Zn	n.a.	27	45	37	24	99.4	109	91.9	102	130	107	n.a.	n.a.	26
Ga	n.a.	14	11	11	11	9.91	12	9.42	8.09	13	11.9	n.a.	n.a.	9.2
Ge	n.a.	n.a.	n.a.	n.a.	n.a.	1.75	1.32	1.27	1.29	1.54	1.33	n.a.	n.a.	
Cs	n.a.	2.4	1.1	1.1	2.3	2.61	7.24	4.56	2.98	6.63	5.56	n.a.	n.a.	1.4
Ba	227	32	32	39	78	18.90	138.00	51.70	45.10	80.80	28.70	n.a.	n.a.	41

(*continued*)

Table 1 (*continued*)

Group	Group 1	Group 2												
Rock type	Grabbro	Basalt	Gabbro	Gabbro	Gabbro	Gabbro	Gabbro	Gabbro	Gabbro	Gabbro	Gabbro	Gabbro	Gabbro	Doleritic rock
Grain size	medium-coarse	fine	coarse	coarse	coarse	coarse	coarse	coarse	coarse	coarse	coarse	coarse	coarse	medium-fine
Samples	TC006	TC004-1	TC007-1	TC008-1	TC001-1	CX-1	CX-2	CX-3	CX-4	CX-5	CX-6	D91001	D91002	TC006-1
Y	n.a.	13.53	20.24	19.4	13.17	12.90	14.20	10.50	9.51	12.70	11.20	n.a.	n.a.	17.14
La	n.a.	0.79	1.19	1.35	0.92	0.72	0.66	0.59	0.47	0.34	0.45	3.9	7.7	5.41
Ce	n.a.	2.29	3.41	3.79	3	2.37	2.15	1.39	1.3	0.95	1.29	8.8	14	10.18
Pr	n.a.	0.45	0.67	0.72	0.53	0.45	0.41	0.24	0.23	0.2	0.24	1.1	1.9	1.37
Nd	n.a.	2.56	3.8	4.01	2.75	3.09	2.94	1.87	1.71	1.67	1.86	4.8	7.3	5.79
Sm	n.a.	1.14	1.53	1.47	1.17	1.3	1.35	0.89	0.76	0.91	0.89	1.3	1.8	1.63
Eu	n.a.	0.49	0.57	0.58	0.52	0.56	0.32	0.38	0.41	0.41	0.42	0.56	0.78	0.63
Gd	n.a.	1.66	2.49	2.42	1.68	1.99	2.18	1.55	1.37	1.64	1.58	2.1	2.3	2.14
Tb	n.a.	0.35	0.52	0.5	0.33	0.39	0.44	0.32	0.29	0.35	0.33	0.41	0.44	0.39
Dy	n.a.	2.38	3.59	3.48	2.4	2.78	3.15	2.24	2.04	2.61	2.45	2.9	2.9	2.56
Ho	n.a.	0.51	0.79	0.77	0.52	0.63	0.71	0.48	0.47	0.61	0.56	0.62	0.6	0.55
Er	n.a.	1.52	2.39	2.31	1.53	1.88	2.07	1.49	1.41	1.8	1.68	1.81	1.7	1.59
Tm	n.a.	0.26	0.39	0.38	0.26	0.27	0.3	0.23	0.21	0.26	0.25	0.27	0.26	0.26
Yb	n.a.	1.58	2.49	2.45	1.62	1.85	2.03	1.57	1.49	1.76	1.74	1.7	1.6	1.6
Lu	n.a.	0.24	0.39	0.39	0.25	0.3	0.32	0.25	0.25	0.28	0.27	0.26	0.25	0.26
Rb	10	2.8	5.7	8.8	18	5.55	24.10	17.50	13.70	27.70	22.00	n.a.	n.a.	5.2
Sr	50	104	206	192	128	141.00	136.00	172.00	189.00	89.90	154.00	n.a.	n.a.	179
Hf	n.a.	0.8	0.9	0.6	0.6	0.91	0.99	0.62	0.54	0.59	0.64	n.a.	n.a.	0.8
Sc	n.a.	28	32	32	24	32.90	34.70	31.80	31.50	38.70	38.20	n.a.	n.a.	12
Nb	n.a.	3.7	2.1	3.7	4.3	0.48	0.50	0.42	0.35	0.32	0.42	n.a.	n.a.	3.3
Ta	n.a.	<0.5	<0.5	<0.5	0.5	0.03	0.03	0.02	0.02	0.02	0.03	n.a.	n.a.	0.66
Pb	70	3.7	9.7	9.2	2.9	n.a.	n.a.	n.a.	n.a.	n.a.	n.a.	n.a.	n.a.	2
Th	n.a.	2.7	3.1	3.9	2.2	0.02	0.03	0.03	0.02	0.03	0.03	n.a.	n.a.	5.9
U	n.a.	0.81	0.59	0.49	0.68	0.66	0.07	0.11	0.06	0.34	0.26	n.a.	n.a.	0.96
Ti	2794.1	3410.2	4013.4	4274.9	3446.1	3360.0	3720.0	2460.0	2340.0	3000.0	2820.0	n.a.	n.a.	2749.4

Major elements in wt.%, trace elements in ppm; *n.a.* not analysed; Total, volatile-free; $FeO^{*} = FeO + Fe_2O_3$; data for samples CX1 to CX6 from *Li* et al. (2002); $Mg^{\#} = 100 * [Mg/(Mg + 0.9 * Fe_{total})(atomic)$

contains a mylonitic texture with amphibole porphyroclast showing undulose extinction and fish-like shape (Fig. 3g). Despite the intense metamorphism and alteration, some medium to coarse-grained samples sometimes preserve gabbroic to diabasic textures (Fig. 3h).

Collectively, the protoliths for the Tunchang area metabasites probably are composed of coarse-grained gabbroic rocks, medium to fine-grained gabbroic rocks and fine-grained and/or massive pillowed lava, which are crosscut by diabasic to gabbroic dykes and in turn are covered by volcanioclastic sediments. We therefore suggest that these rocks most likely represent the upper layers of an unkown ophiolite or an incomplete, dismembered ophiolite body (Fig. 2b).

Data sources and analytical procedures

Twenty-three fresh surface samples were taken from the metabasite body in Tunchang area, East-central Hainan Island. All samples were analyzed for major elements nineteen samples for trace- and rare earth elements, and sixteen samples for Sr-Nd isotopes. The analytical results are presented in Tables 1 and 2. Major element abundances for 23 samples were determined at Institute of Geochemistry, Chinese Academy of Sciences, using X-ray fluorescence (XRF) and wet chemical methods. Trace element concentrations were measured using Inductively Coupled Plasma-Atom Emission Spectrometry (ICP-AES) and Inductively Coupled Plasma-Mass Spectrometry (ICP-MS). The analytical precision (in relative standard deviation) is usually $<3\%$ for major elements except H_2O^+, $<4\%$ for REEs and Y, and 3–7% for other trace elements.

Sr and Nd isotopic analyses were carried out at the Isotopic Laboratory of the Yichang Institute of Geology and Mineral Resources, following methods described by *Ma* et al. (1998). All the isotopic determinations were performed on a Finnigan MAT261 surface ionization mass spectrometer equipped with 7 Faraday cup collectors. $^{87}Rb/^{86}Sr$ and $^{147}Sm/^{144}Nd$ ratios were determined to precisions of $\pm 0.7\%$ and $\pm 0.1\%$, respectively. Parameters used for calculations include: $^{143}Nd/^{144}Nd$ ratio of CHUR at the present time $= 0.512638$, $^{147}Sm/^{144}Nd$ ratio of CHUR at the present time $= 0.1967$. The DM values for Nd are $(^{143}Nd/^{144}Nd)_{Today} = 0.51315$, $(^{147}Sm/^{144}Nd)_{Today} = 0.2137$. The decay constants used were: $\lambda\ (^{87}Rb) = 0.0142 Ga^{-1}$ and $\lambda\ (^{147}Sm) = 0.00654\ Ga^{-1}$.

Results

Bulk rock geochemistry

Most of the Tunchang area metabasites have silica values (*volatile-inclusive*) typical of basaltic rocks (Table 1). The ratios of Nb/Y and Zr/TiO_2 classify them as dominant sub-alkaline basalts with minor andesitic compositions (Fig. 4a). The low ratios of Ti/Y and Nb/Y are characteristic of tholeiitic basalts (Fig. 4b). Based on the criteria of Ti/Y <410 and Zr/Y <6 (*Erlank* et al., 1988), these rocks are further classified as low-Ti tholeiites. Several samples (i.e. TC001, TC002, TC003, TC004 and TC006) with higher SiO_2 contents (55–57 wt.%), which might most appropri-

Table 2. *Sr and Nd isotope compositions of bulk rocks, and amphibole and plagioclase separates from the Tunchang area metabasites in the East-central Hainan Island, South China*

Sample	Rb (ppm)	Sr (ppm)	$^{87}Rb/^{86}Sr$	Error (%)	$^{87}Sr/^{86}Sr$	Error (%)	$^{87}Sr/^{86}Sr_I$	Sm (ppm)	Nd (ppm)	$^{147}Sm/^{144}Nd$	$^{143}Nd/^{144}Nd$	$\pm 2\sigma$	$\varepsilon_{Nd}(t)$	Note	Group
YSY-01	2.074	63.16	0.09465	0.08	0.70703	0.004	0.705288	1.095	2.754	0.2404	0.513078	0.000008	+6.75	BR	Group 1
YSY-02	2.235	103.9	0.06197	0.13	0.70745	0.002	0.707159	1.079	2.684	0.2432	0.512949	0.000008	+4.11	BR	
YSY-03	4.893	121.1	0.1165	0.14	0.7079	0.003	0.702393	1.035	2.606	0.2403	0.512953	0.000009	+4.31	BR	
YSY-04-1	24.83	298.9	0.2395	0.56	0.70853	0.001	0.707049	0.9075	2.212	0.2482	0.513033	0.000009	+5.54	BR	
YSY-04-2	9.229	198.1	0.1343	0.18	0.70792	0.002	0.704630	0.8294	2.063	0.2433	0.512994	0.000008	+4.98	BR	
12B-07	0.5263	74.24	0.02044	0.12	0.70637	0.004								BR	
12B-08	0.927	165.1	0.17978	0.01	0.706509	0.0041	0.705665							BR	
12B-09	0.81	126.2	0.16276	0.01	0.706111	0.0034	0.705347							BR	
YSY-05-1	13.02	31.3	1.2	0.36	0.71099	0.003	0.699332	0.8793	2.271	0.2343	0.512830	0.000012	+2.16	BR	
YSY-05-2	15.25	29.48	1.493	0.33	0.71456	0.002	0.708243	1.024	2.521	0.2458	0.512935	0.000008	+3.73	BR	
YSY-06	11.26	163.1	0.119	0.25	0.70882	0.004	0.708261	1.689	3.924	0.2604	0.513085	0.000011	+6.04	BR	
TC001-1	18	128	0.3663	0.02	0.708317	0.002	0.706596							BR	Group 2
TC004-1	2.8	104	0.0447	0.02	0.706893	0.0015	0.706683							BR	
TC007-1	5.7	206	0.0706	0.02	0.70838	0.0016	0.708048	1.53	3.8	0.2834	0.513069		+4.76	BR	
TC008-1	8.8	128	0.122	0.02	0.708466	0.0015	0.707893							BR	
TC001-1 (AHL)	31.6	327.6	0.3093	0.02	0.708346	0.0015	0.706893	0.7	3.1	0.1365	0.512925		+8.14	Amp	
TC007-1 (AHL)	5.3	307.4	0.0552	0.02	0.70841	0.0014	0.708151	1.7	6.4	0.1606	0.512966		+7.93	Amp	
TC007-1 (Pl)	21.6	606	0.1126	0.02	0.708631	0.0013	0.708102							Pl	
TC008-1 (Pl)	21.7	562.2	0.1213	0.02	0.708659	0.0016	0.708089							Pl	
TC008-1 (AHL)	3.5	181.5	0.065	0.02	0.708632	0.0031	0.708327							Amp	
TC006-1	5.2	179	0.2698	0.02	0.708751	0.0014	0.707484							BR	
TC006-1 (AHL)	37.8	439.5	0.2669	0.02	0.708775	0.0016	0.707521	1.5	6.6	0.1374	0.512669		+3.11	Amp	
CX1 to CX6 (total six samples)								0.87–1.40	1.80–3.15	0.2445–0.3167	0.513083–0.513243		+6.70–+6.75	BR	

BR Bulk rock; *Amp* amphibole by magnetic separator and heavy liquid (AHL); *Pl* plagioclase by heavy liquid. An age of 330 Ma (*t*) from *Li* et al. (2002) is used to calculate initial Sr and Nd isotopic values. Also, data for samples CX1 to CX6 (total six samples) are cited from *Li* et al. (2002)

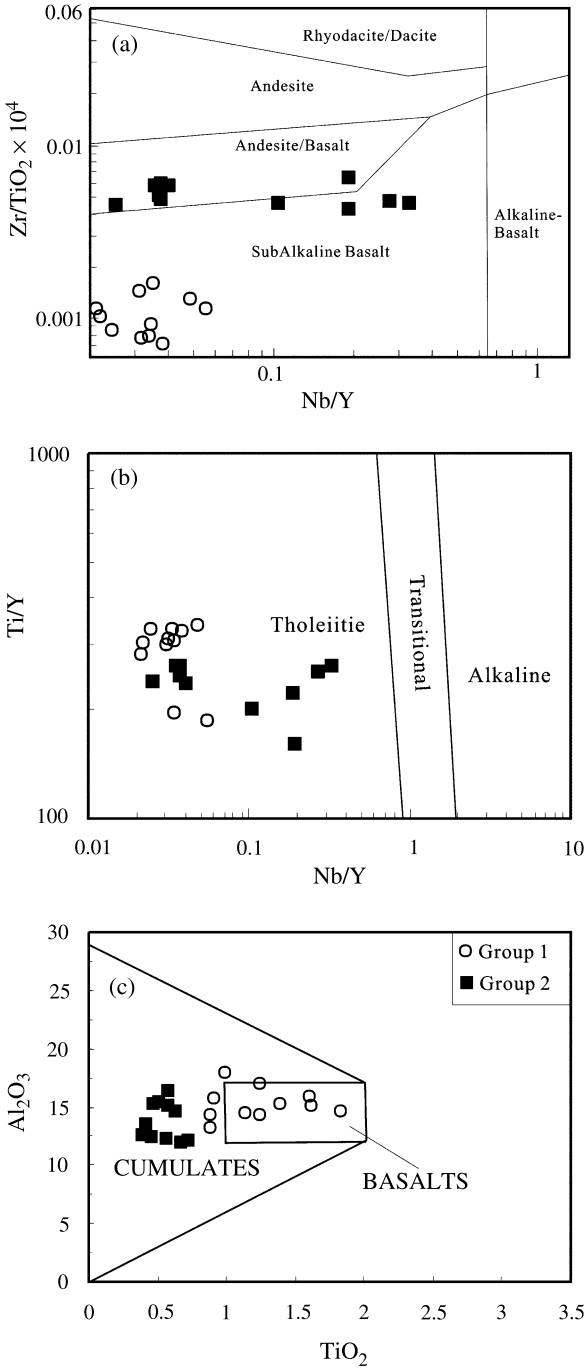

Fig. 4. (**a**–**c**) Discrimination diagrams for the Tunchang area metabasites, indicating that they are low-Ti tholeiites (**a** and **b** after *Winchester* and *Floyd*, 1977; *Erlank* et al., 1988), and can be interpreted as cumulates (dominated by Group 2) and basalts (dominated by Group 1) (**c** based on *Pearce*, 1983). Some data for Group 2 are from *Li* et al. (2002)

ately be termed basaltic andesites, probably had been affected by post-magmatic alteration and/or metamorphism.

The Tunchang area metabasites further can be classified into two groups, i.e. Groups 1 and 2, based on Figs. 4c and 5. Group 1 contains basaltic rock-dominated, basaltic and gabbroic rocks. These rocks range in mg-number ($Mg^{\#}$) from

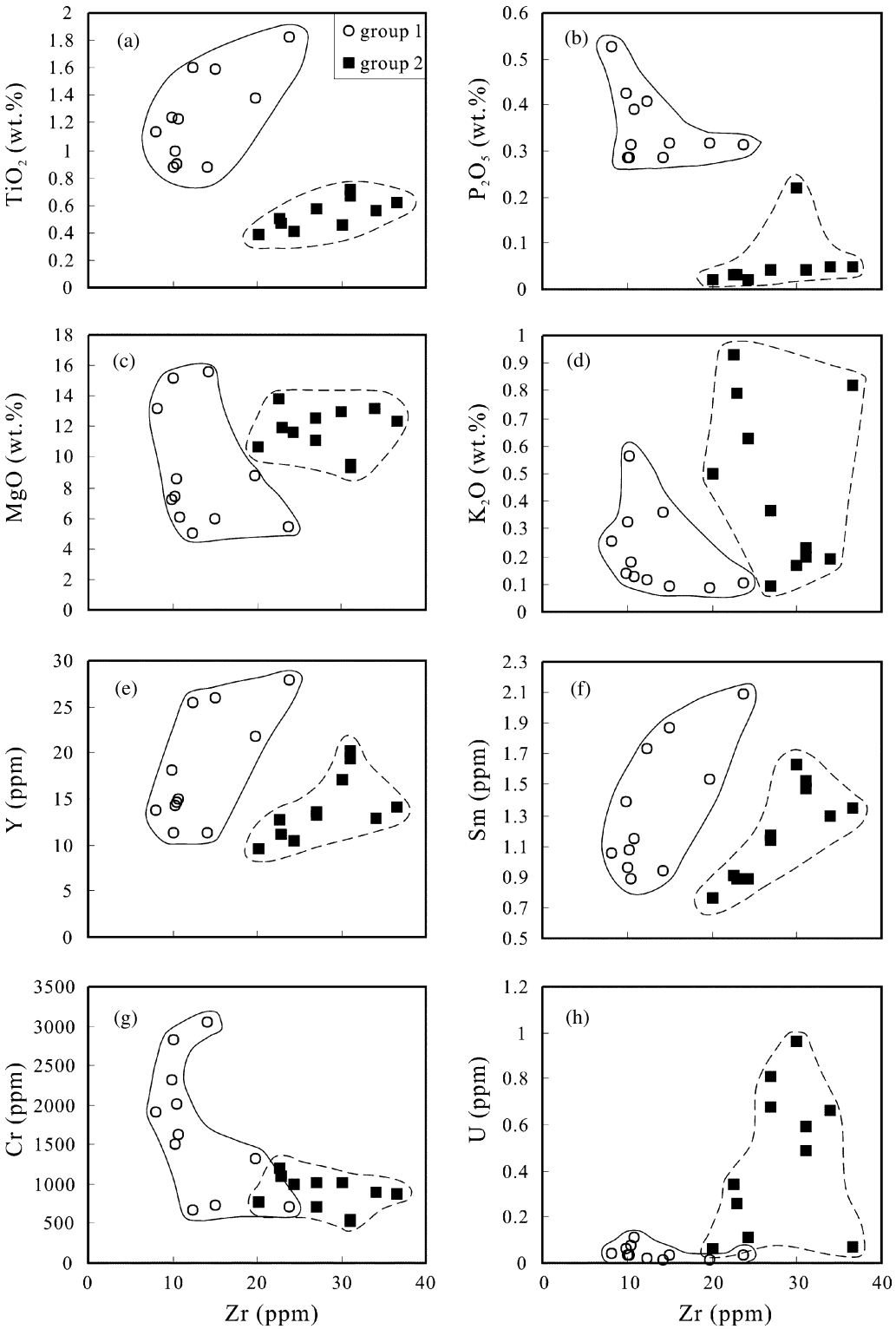

Fig. 5. Plots of selected major and trace elements *vs.* Zr for the Tunchang area metabasites. Some data for Group 2 are from *Li* et al. (2002). These diagrams show that the metabasites can be discriminated into two groups with limited overlap, i.e., low-Ti/P-type (Group 1) and high-Ti/P-type (Group 2)

55 to 82, MgO from 5.0 to 15.6 wt.% (generally between 5.0 and 10 wt.%), SiO_2 from 51.3 to 57.9 wt.%, TiO_2 from 0.38 to 1.82 wt.%, FeO^* (= FeO + Fe_2O_3) from 4.36 to 8.68 wt.%, Al_2O_3 from 13.1 to 17.9 wt.%, and CaO from 9.0 to 14.4 wt.% (Table 1, *volatile free*). K_2O contents are low (0.10–0.56 wt.%), whereas P_2O_5 are high (0.28–0.53 wt.%) in these rocks. Also, the Group 1 rocks are characterized by relatively low Zr (10–24 ppm), Th (0.03–0.18 ppm) and U (0.02–0.11 ppm) abundances as well as relatively high Sc (41–50 ppm), Cr (527–3055 ppm), V (293–524 ppm) and Ni (105–514 ppm) concentrations. The high P_2O_5 content for this Group probably is related to accumulation of apatite, whereas two samples (YSY-02, YSY-06) with high TiO_2/Gd ratios (>0.50) can be designated as ilmenite cumulates (e.g., *Coogan* et al., 2001).

Group 2 contains gabbroic rock-dominated, gabbroic, diabasic and basaltic rocks. Generally, these rocks have mg-numbers ranging from 69 to 78 with MgO contents varying from 8.0 to 13.8 wt.% (Table 1, *volatile free*). Compared to the Group 1 rocks, the Group 2 samples are lower in TiO_2 (0.39–0.80 wt.%), P_2O_5 (0.02–0.25 wt.%) and SiO_2 (44.7–55.0 wt.%), but higher in K_2O (generally >0.20 wt.% and up to 0.93 wt.%) (Table 1, *volatile free*). These rocks, which have more affinities to cumulates (Fig. 4c), also have higher Zr (27–36.5 ppm), Th (0.02–5.9 ppm) and U (0.06–5.9 ppm) and lower Sc (24–39 ppm), Cr (536–

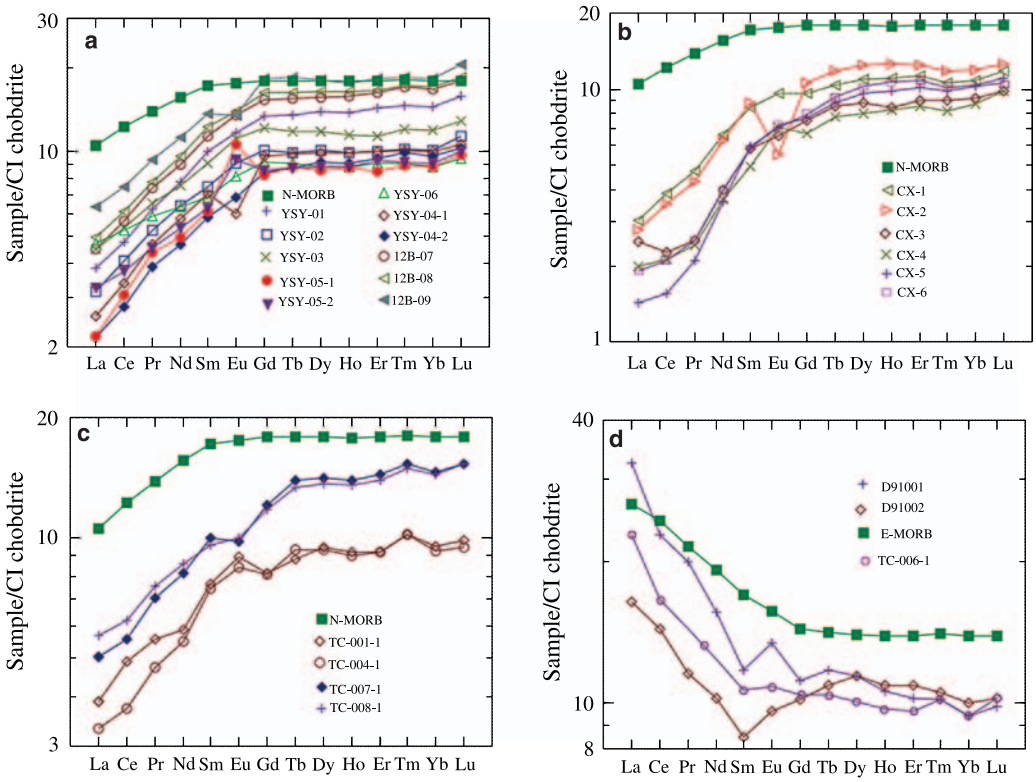

Fig. 6. Chondrite-normalized REE spectra for the Tunchang area metabasites. CI Chondrite REE compositions, N- and E-MORB values are from *Sun* and *McDonough* (1989), data in **b** are from *Li* et al. (2002)

1192 ppm), V (143–260 ppm) and Ni (160–382 ppm) concentrations, in comparison with the Group 1 rocks. As a result, Group 2 shows higher Al_2O_3/TiO_2 (17–36) and Zr/Y (1.53–2.64) ratios but lower Ti/Zr (88–133) ratio than Group 1 (8–18, 0.48–1.25 and 156–634, respectively). Because the poikilitic amphiboles are generally low in K_2O (<0.1 wt.%, *Xu* et al., 2006), the K-enrichment probably is related to decreasing degree of partial melting with increasing depth in respond to smaller amount of water released from the downgoing slab in subduction-related settings (*Faure*, 2001).

Most of the studied rocks display extremely low REE concentrations (an overall enrichment of 5–12 times chondrite, *Sun* and *McDonough*, 1989) and strongly LREE-depleted patterns ($La/Yb_{cn} = 0.14–0.53$) (Table 1 and Fig. 6), being comparable to those of the Oman ophiolites (*Kelemen* et al., 1997) and the northwestern Ontario LREE-depleted arc basalts (*Hollings* and *Kerrich*, 2004). Very similar patterns to those of gabbroic cumulate rocks from various ophiolites (*Benoit* et al., 1996) and the recent oceanic crust (*Constantin*, 1999) also have been reported. Two samples (YSY05-1, YSY05-2) in Group 1 show larger positive Eu anomalies ($Eu^*/Eu = 1.20–1.27$), indicating the presence of plagioclase accumulation.

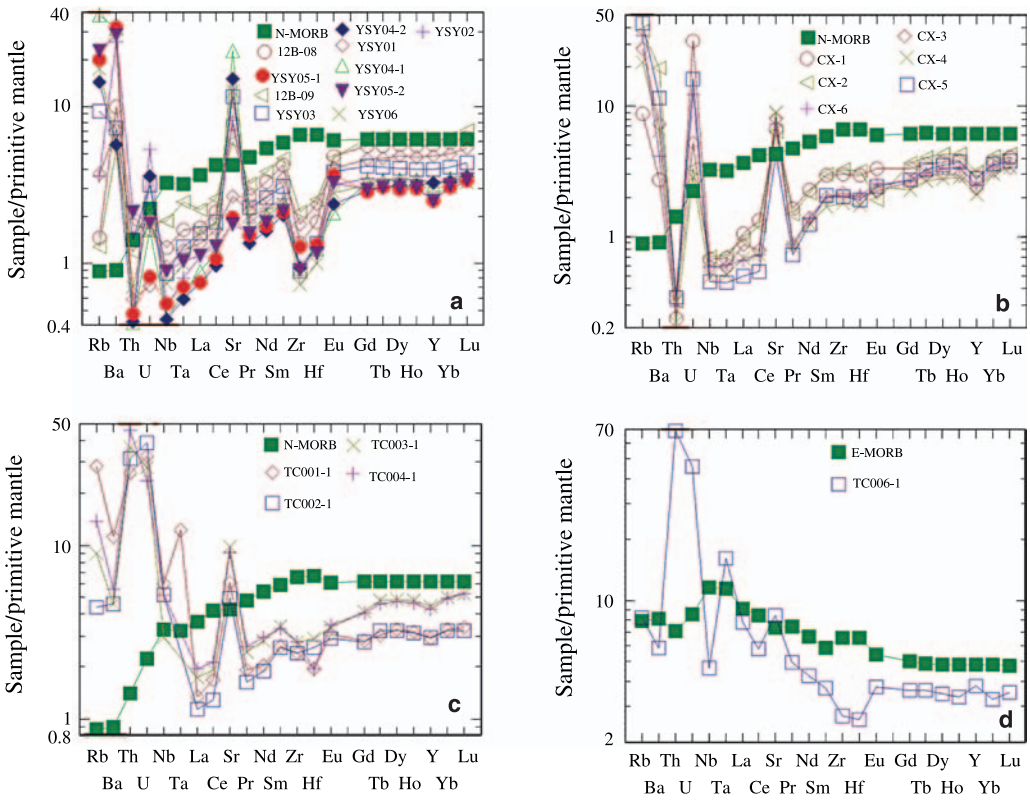

Fig. 7. Primitive mantle-normalized multi-element plots for the Tunchang area metabasites. Primitive mantle normalization values, N- and E-MORB values are from *Sun* and *McDonough* (1989), and data for samples CX1 to CX-6 in Group 2-A from *Li* et al. (2002)

However, three samples D91001, D91002 and TC006-1 in Group 2 (Fig. 6d), which most likely represent medium to coarse-grained diabasic rocks, show concave-up, slightly LREE-enriched patterns ($La/Yb_{cn} = 1.65–3.45$) together with slightly positive Eu anomalies, comparable to those of the E-MORBs (*Sun* and *McDonough*, 1989).

The Primitive Mantle-normalized spidergrams (Fig. 7) reflect that most of the studied rocks generally are enriched in LILEs such as Ba, Rb, Sr and U, and strongly depleted in HFSEs such as Nb, Ti, Y, Zr, Hf and Th, relative to the N-MORBs and Primitive Mantle (*Sun* and *McDonough*, 1989). Despite an overall similarity in the Fig. 7, most of the Group 1 rocks are relatively enriched in Ti and Y, and depleted in Zr and Hf, in comparison with most of the Group 2 samples. Positive Ti anomalies displayed by the Group 1 samples are consistent with their oxide-rich nature, whereas negative to positive Zr-Hf anomalies for the studied rocks probably reflect a two-stage melting history in subarc mantle wedge (e.g., *Manikyamba* et al., 2004). The sample TC006-1 in Group 2 exhibits similarities to E-MORBs (Fig. 7), but still can be discriminated from the latter by its remarkably low concentrations of incompatible elements and its Th and U spikes.

Sr-Nd isotopes

We have also analyzed the Sr-Nd isotopic compositions of sixteen samples (Table 2). The Tunchang area metabasites have $^{147}Sm/^{144}Nd$ ratios ranging from 0.2343 to 0.3167 and $^{87}Sr/^{86}Sr_i$ values ranging from 0.699332 to 0.708243 and relatively low $\varepsilon_{Nd}(t = 330\,Ma)$ values ranging from +2.16 to +6.75, which are comparable to those of island arc basalts (*Faure*, 2001).

Groups 1 and 2 metabasites are also distinct regarding their Sr-Nd isotopic compositions. Compared to the Group 1 rocks (0.512830–0.513078), the Group 2 samples have higher measured $^{143}Nd/^{144}Nd$ ratios (0.512925–0.513243) (Table 2). The corresponding values of $\varepsilon_{Nd}(t)$ and $^{87}Sr/^{86}Sr$ are + 4.76 to +6.75 and 0.70611 to 0.70875, respectively for the Group 2, and +2.16 to +6.75 and 0.70611 to 0.71456, respectively for the Group 1. These values likely indicate that the magmatic source is geochemically heterogeneous, due to involvement of an enriched component into the depleted mantle source, or contributions of small amounts of old crustal materials and/or both subducted sediments and altered oceanic crust. Alternatively, the source could have undergone variable degree of partial melting and/or fractional crystallization (see below).

Discussion

Alteration and metamorphism

The Tunchang area metabasites probably had been affected to varying degrees by sea-floor alteration, (regional/thermal) metamorphism and deformation, based on the petrographical and mineralogical observations, and microstructures. These later processes may have disturbed the original abundance of some elements. Hence, before using the geochemical data to interpret the petrogenesis and tectonic setting, we need to confirm whether all elements still reflect the original magmatic com-

position, or whether they have been remobilized during the processes of alteration and metamorphism.

Because of its relative immobility during alteration and metamorphism, the incompatible element Zr has been frequently used as reference to infer the mobilities of major-, trace- and rare earth-elements (*Rolland* et al., 2002 and references therein). Based on the correlation of Zr with main- and trace elements (Fig. 5), we thus interpret the differences in geochemical composition between Groups 1 and 2 as being due to magmatic processes rather than to alteration processes. The relatively low LOI values for Group 1 (2.35–4.09 wt.%) and Group 2 samples (1.52–3.29 wt.%; Table 1) also indicate that hydrothermal alteration was not intense. Several samples have extremely high abundances of Rb (>20 ppm) and Cs (>4 ppm), probably indicating low-temperature alteration effects (e.g., *Hart* and *Staudigel*, 1982).

In order to check whether hydrothermal alteration had any effects on the Nd and Sr isotopic compositions, a representative sample (YSY04-1) characterized by extremely high Sr and Zn, and high Ba, Rb and LOI contents (Table 1) has been chosen. Its $\varepsilon_{Nd}(t)$ ratio of +5.54 is within the range of other samples (+2.16 to +6.75, Table 2). Hence we conclude that neither metamorphism nor low temperature alteration significantly affected the Nd isotopic system of the studied rocks. The same sample also shows an $^{87}Sr/^{86}Sr_i$ value as high as 0.707049 (Table 2). These higher $^{87}Sr/^{86}Sr_i$ values could reflect the effect of seawater alteration, since the $^{87}Sr/^{86}Sr_i$ *vs.* $\varepsilon_{Nd}(t)$ diagram (Fig. 8) clearly indicates that the studied samples had been severely altered by seawater. However, an exceptional sample is the sample YSY05-1 in Group 1, which not only has the lowest $\varepsilon_{Nd}(t)$ value (+2.16), but also has the lowest $^{87}Sr/^{87}Sr_i$ ratio (0.699332) (Table 2). A depleted mantle source modified by a relatively enriched component (e.g., a slab-derived fluid and/or melt) could yield such a low $\varepsilon_{Nd}(t)$ value (*see discussion below*), whereas post-magmatic enrichment in Rb likely accounts for the extremely low $^{87}Sr/^{87}Sr_i$ ratios (*Brewer* and *Menuge*, 1998). This interpretation is supported by the following characteristics; the same sample has the highest content of MgO (15.56 wt.%), moderately high contents of P_2O_5 (0.28 wt.%) and TiO_2 (0.87 wt.%),

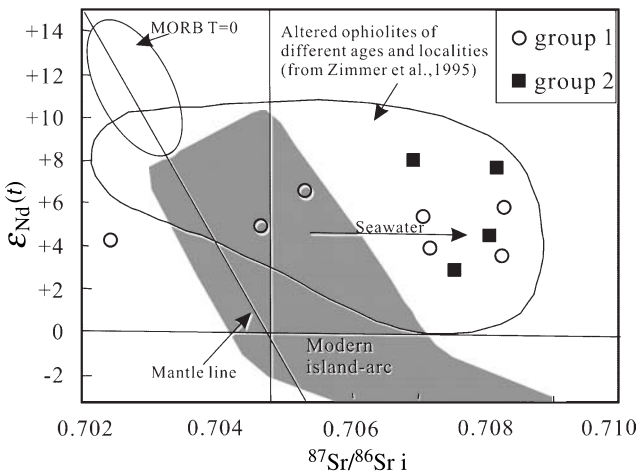

Fig. 8. Diagrams of $\varepsilon Nd(t = 330\,Ma)$ against $^{87}Sr/^{86}Sr_i$ after *Zimmer* et al. (1995) for the Tunchang area metabasites

and a moderately high ratio of Rb/Sr (0.3, Table 1). The REE patterns of the studied rocks (Fig. 6), which are not randomly spiky but yield relatively smooth patterns, highlight the fact that alteration and/or metamorphism did not significantly modify the REE characteristics.

Therefore, the general immobility of REEs, HFSEs and TEs (transition metals) during alteration and/or metamorphism gives confidence to their use as petrogenetic and geotectonic indicator elements for the studied rocks. Those samples (e.g., TC001, TC003 and TC004) that show rather high contents in SiO_2 and Na_2O (Table 1) suggest that silicification and/or other types of alteration (e.g., sea-floor alteration) remain important and probably led to redistribution of some mobile elements. To avoid misinterpretations caused by such alteration effects, only the most representative samples that show minor major and trace element variations and deviation from the differentiation trend of the series have been selected for isotopic analyses.

Crustal contamination

HFSE and REE concentrations in the studied rocks (Table 1) do not reflect crustal contamination. The low Ce/Yb ratios (generally <2.2) support that crustal contamination is negligible in petrogenesis of the studied rocks (e.g., *Hawkesworth* et al., 1993). This can also be seen in the Yb *vs.* Ce plot (Fig. 9), where the studied rocks define a similar trend as intra-oceanic arc basalts from the South Sandwich Islands and Tonga-Kermadec arcs. The higher positive initial ε_{Nd} values further imply the mantle-derived magmatism without significant contribution from old continental crust in the generation processes of their protoliths, being consistent with the presence of pillow basalts (Fig. 3c) indicative of an oceanic environment

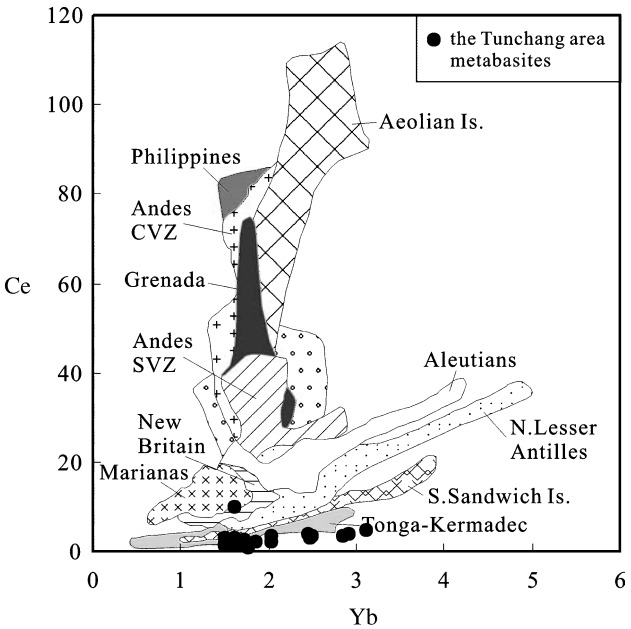

Fig. 9. Plot of Ce *vs.* Yb for the Tunchang area metabasites. Fields for various intraoceanic arcs are from *Manikyamba* et al. (2004), some data for Group 2 are from *Li* et al. (2002)

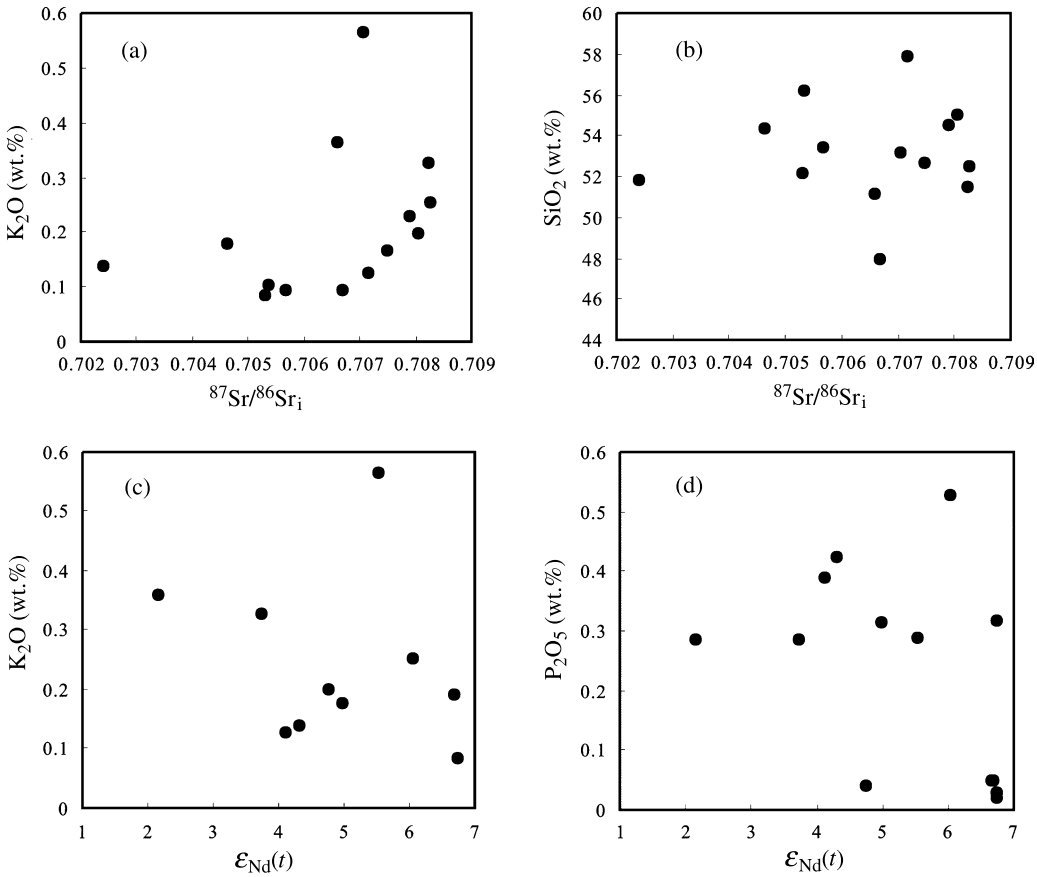

Fig. 10. Plots of $^{87}Sr/^{86}Sr_i$ and $\varepsilon_{Nd}(t)$ versus K_2O, P_2O_5 and SiO_2 contents of the Tunchang area metabasites. Note the weak correlation between $^{87}Sr/^{86}Sr_i$ and K_2O, and no correlations between $^{87}Sr/^{86}Sr_i$ and SiO_2, between $\varepsilon_{Nd}(t)$ and K_2O, and between $\varepsilon_{Nd}(t)$ and P_2O_5

for their generation. Some similarities in trace elements and Sr-Nd isotopes to the oceanic crust beneath Canary Islands (*Hoernle*, 1998) and from DSDP-ODP Sites 417/418 in the western Atlantic (*Staudigel* et al., 1995) reflect that the protoliths for the studied rocks were derived primarily from mantle sources rather than crustal assimilation. The weak correlation between $^{87}Sr/^{86}Sr_i$ and K_2O, the lack of correlation between $^{87}Sr/^{86}Sr_i$ and SiO_2, and no correlations between $\varepsilon_{Nd}(t)$ *vs.* P_2O_5 and K_2O (Fig. 10) further imply that contamination of magma by crustal materials and later alteration by crustal or seawater-derived fluid are extremely minor (*Lu* et al., 1997). Obviously, crustal contamination is highly unlikely to have played a major role in generating magmas for the protoliths of the Tunchang area metabasites.

Magmatic trend

The differences in the ratios of incompatible elements between Group 1 and 2 imply that they derived from different mantle sources or from a heterogeneous

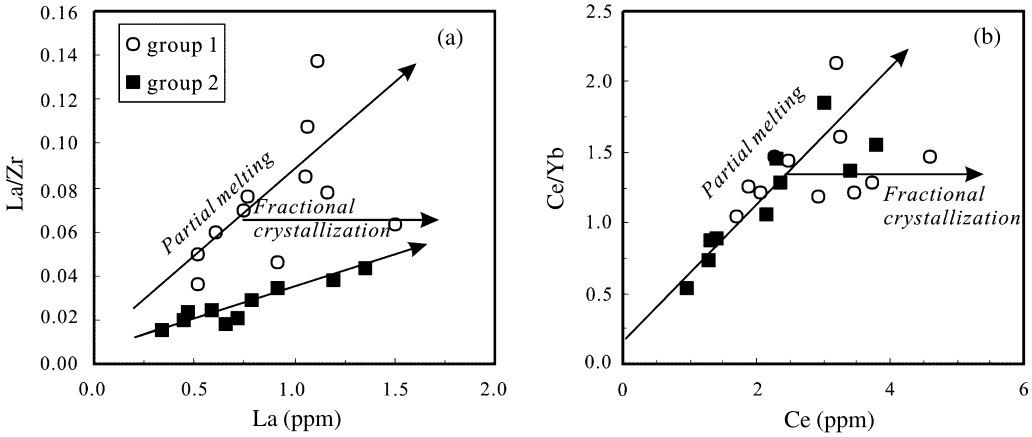

Fig. 11. Diagrams of La *vs.* La/Zr (**a**) and Ce *vs.* Ce/Yb (**b**) for the Tunchang area metabasites, indicating that partial melting of variable degree might have played a key role in generating magmas for the studied rocks; some data for Group 2 are from *Li* et al. (2002)

mantle source, and/or from various degrees of partial melting (e.g., *Pearce* and *Norry*, 1979). The overall similarity in trace- and rare earth elements, and Sr-Nd isotopes between Groups 1 and 2, however, does not support the presence of two mantle sources. The restricted values of Tb/Yb (±0.21) and La/Yb (0.20–0.57), and the plots of La *vs.* La/Zr and Ce *vs.* Ce/Yb (Fig. 11) are rather consistent with variable degrees of partial melting of a common, heterogeneous mantle source, which contained zero to very small amounts of residual garnet and had a primitive mantle abundance of the REE (*Sun* and *McDonough*, 1989), might have played a key role in generating protolith magmas of the studied metabasites. The extremely low HFSE and REE contents, together with the strongly LREE-depleted patterns, further reflect higher degrees of partial melting, e.g., up to 20%–30%, as proposed by *Cullers* and *Graf* (1984), from the residue of a depleted primitive mantle that had previously undergone extraction event of parental melts. Such high melting rates most likely resulted from melting in a high temperature shallow fore-arc mantle wedge and/or by decompression to shallower levels along a particular adiabatic ascent path, which is common beneath young intraoceanic subduction-related systems (e.g., *Tatsumi* and *Eggins*, 1995).

The good correlation within each single group, between Zr and many major and trace elements (Fig. 5) still reveals fractional crystallization probably as an evolutionary process for the studied rocks. A significant geochemical feature is that all the studied samples have high concentrations of Cr and Ni (Table 1). *Magganas* (1990) suggested that Cr-spinel and Cr-clinopyroxene do not have significant Ni contents. Neither the petrographic observation nor the microprobe analysis (*Xu* et al., 2006) shows the occurrence of chromite, spinel and garnet in the studied rocks, indicating that Cr-bearing clinopyroxene and/or olivine were the early crystallizing phases (*Halkoaho* et al., 2000). This inference is consistent with the data array on the Al_2O_3/TiO_2 *vs.* Ti plot (Fig. 12a), where the data define a line mainly parallel to the clinopyroxene vector, pointing out the main influence of this phase

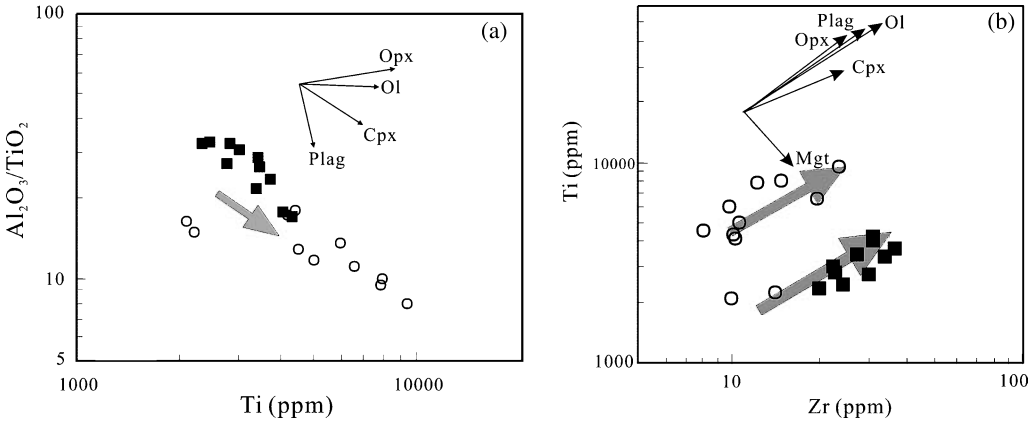

Fig. 12. Fractional crystallization trends for mineral phases shown in diagrams of Ti *vs.* Al_2O_3/TiO_2 (**a**) and Zr *vs.* Ti (**b**) for the Tunchang area metabasites. *Opx* orthopyroxene; *Plag* plagioclase; *Ol* olivine; *Cpx* clinopyroxene; *Mgt* magnetite; some data for Group 2 are drawn from *Li* et al. (2002)

during fractional crystallization. However, the plot of Zr *vs.* Ti (Fig. 12b) that identifies two trends respectively subparallel to the olivine + clinopyroxene vectors or the olivine + clinopyroxene ± plagioclase vectors, more likely reflects the trends produced commonly by variable degree of partial melting and fractional crystallization.

Summarizing, the parental melts to the Tunchang area metabasites were derived from a heterogeneously depleted mantle source, which previously might have undergone melt extraction events. The protoliths for these rocks most likely were generated by variable degree of partial melting and late-stage crystal fractionation. The magmatic processes that formed the protoliths of the studied rocks are very similar to those in the Troodos ophiolitie (for a review see *Coogan* et al., 2003).

Source metasomatism and SZ components

It is now widely accepted that arc magmas generated by melting of the oceanic upper mantle above a subducting slab has been previously modified by LILE-rich fluids and/or melts originating from the sediments and/or the basaltic crust of the subducted slab through metasomatism and reaction (*Gill*, 1981; *Pearce* and *Peate*, 1995; *Tatsumi* and *Eggins*, 1995). The restricted range of the observed initial Nd isotope ratios, together with the strongly LREE-depleted patterns and the absence of alkalic basalts, rules out subcontinental mantle as the source for protoliths of the Tunchang area metabasites (e.g. *La Fléche* et al., 1998). Hence, the enrichment of LILEs in the studied rocks (Fig. 7) most likely can be attributed to dewatering or melting of the subducting slab and metasomatism of the overlying, previously depleted (MORB-like) mantle wedge (*Hole* et al., 1984). The plot of Zr/Y *vs.* Ba/Y (Fig. 13a) also shows a shift towards pelagic sediment compositions for some samples with higher Th/Ce ratios (0.58–1.19) and lower $^{134}Nd/^{144}Nd$ values (Tables 1 and 2), which can be attributed to addition of subducted sediments to the

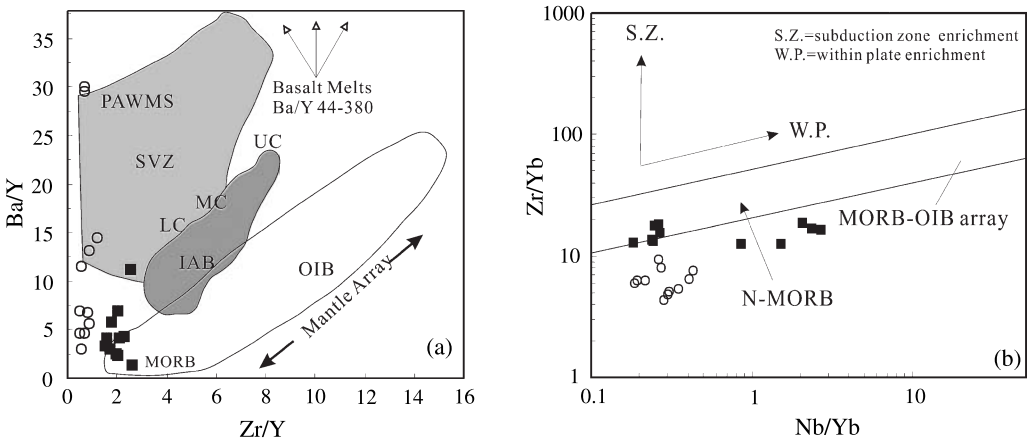

Fig. 13. Plots of Ba/Y *vs.* Zr/Y (**a**) (after *Harry* and *Green*, 1999) and Zr/Yb *vs.* Nb/Yb (**b**) (after *Teklay* et al., 2002; *Manikyamba* et al., 2004) for the Tunchang area metabasites. Average compositions of mid-oceanic ridge MORB and oceanic island OIB basalts in (**a**) after *Sun* and *McDonough* (1989), N-MORB trend in (**b**) from *Pearce* and *Peate* (1995), PAWMS (Pacific Authigenic Weighted Mean Sediment) from *Hole* et al. (1984), points LC, MC and UC (Lower, middle and upper crust) from *Rudnick* and *Fountain* (1995). *SVZ* Andean Southern Volcanic Zone, *IAB* Aleutian Island Arc Basalts, part of data for Group 2 from *Li* et al. (2002)

mantle wedge. However, incompatible element ratios (Nb/Yb *vs.* Zr/Yb in Fig. 13b) clearly designate a few samples plotting within the MORB-OIB array, which implies a contribution from an incompatible elements-enriched melt, as observed in OIB-type mantle sources (e.g. *Teklay* et al., 2002). Considering the petrographical, geochemical and isotopic features of the studied rocks, we attribute the signature of OIB-type mantle sources to the interaction of a mantle plume with the oceanic mantle wedge source prior to subduction (*also see the discussion, below*). Moreover, it is possible that the enrichment processes were related to the presence of a mantle plume leading to the breakup of Rodinia during late Neoproterozoic (*Li* et al., 1999), because the protoliths for the studied rocks have a minimum age of ∼450 Ma (*Xu* et al., 2007).

Petrogenesis

Origin of magma

Some trace element ratios, e.g. La/Sm, Nb/La, Nb/Th and Zr/Nb, appear to characterize most of the Tunchang metabasites as typical N-MORBs (*Sun* and *McDonough*, 1989). These studied rocks, however, show extremely low incompatible element concentrations, relative to N-MORBs (Fig. 7). The relatively low values of ε_{Nd} (330 Ma) (+2.16 to +6.75, Table 2) are also distinct from those for average N-MORBs ($\varepsilon_{Nd}(t) \approx +13$: *Zindler* et al., 1982). As a result, these ε_{Nd} (330 Ma) values, which extend only to 4.6 ε_{Nd} units, are more comparable to those for Proterozoic and modern oceanic arc volcanic rocks (*Teklay* et al.,

2002), implying an intra-ocanic origin. In combination with the low LREE/HREE ratio and the high LILE/HFSE ratio as well as the low Y content (<20 ppm) and the low Ti/V ratio (between 6 and 20), we suggest that the studied rocks derived from an N-MORB-like mantle source slightly enriched in LILEs during a metasomatic event in an oceanic-arc/supra-subduction zone setting. Hence, the shift towards lower ε_{Nd} for some samples, in the absence of underlying crust, may be interpreted as contributions from both subducted sediments and altered oceanic crust (*Faure*, 2001).

Although most of the studied samples display the geochemical characteristics typical of island arc basalts, they appear to have affinities to crustally contaminated komatiitic rocks, and/or to boninitic rocks (Fig. 14). The lack of typical spinifex textures and ultramafic rocks, together with the low MgO contents (generally <16 wt.%), exclude that their protoliths were komatiites (e.g. *Arndt* and *Nisbet*, 1982). However, the studied rocks, which bear signature of an intraoceanic fore-arc component, are obviously such a case. These rocks not only are very depleted in immobile incompatible elements such as Zr and Y, but also extremely enriched in transition metals such as Cr and Ni (Table 1). As a result, these geochemical features are rather similar to those of boninitic rocks of various ages, elsewhere (e.g. *Leybourne* et al., 1997; *Polat* et al., 2002; *Yibas* et al., 2003; *Saccani* and

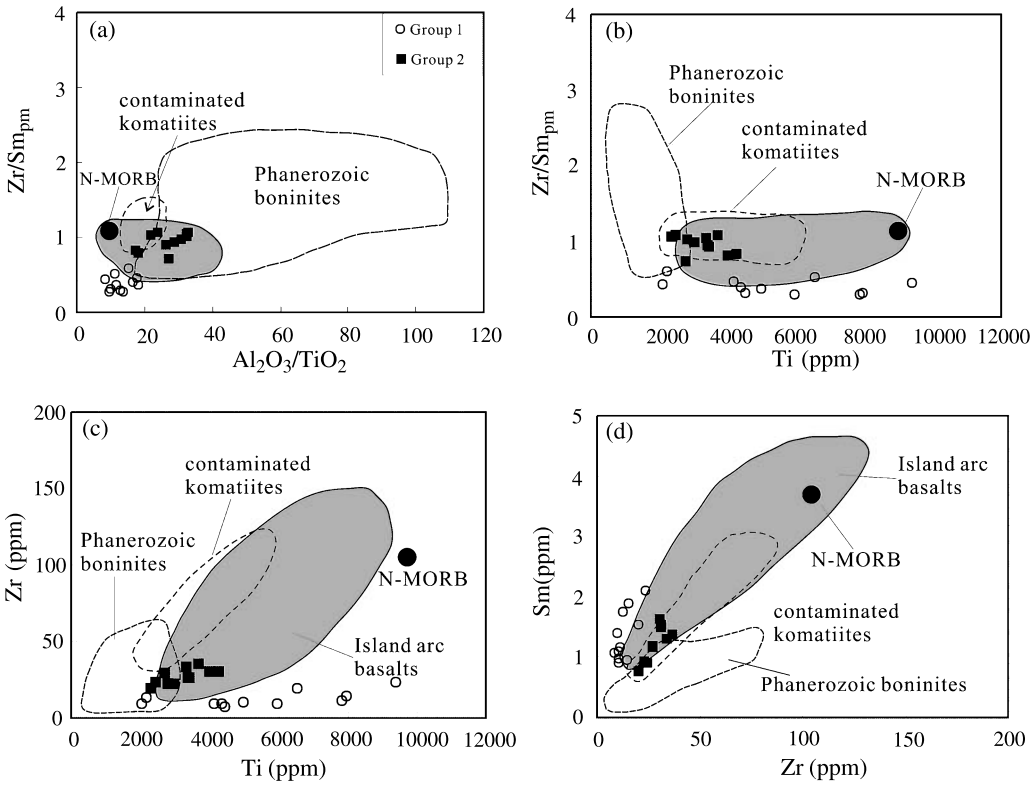

Fig. 14. Al_2O_3/TiO_2 *vs.* Zr/Sm_{pm} (**a**), Ti vs. Zr/Sm_{pm} (**b**), Ti vs. Zr (**c**) and Zr vs. Sm (**d**) variation diagrams for the Tunchang area metabasites (after *Polat* et al., 2002). PM (Primitive mantle) normalization value from *Sun* and *McDonough* (1989), N-MORB values from *Hofmann* (1988), some data for Group 2 are from *Li* et al. (2002)

Photiades, 2004). The sample TC006-1 in Group 2 with low TiO_2 (0.44 wt.%) and concave-up LREE-enriched pattern (Fig. 6) is also comparable to the Adola boninitic rocks from Southern Ethiopia (*Yibas* et al., 2003). Boninites were generally thought to originate as low-pressure partial melts of extremely depleted mantle-wedges, further implying that the studied rocks originated in an intra-oceanic subduction zone-like tectonic setting (e.g. *Bédard*, 1999). However, the high mg-number, and Cr, Co, Ni contents may be indicative of a plume-influenced mantle wedge in the generation of magma for the studied rocks (e.g. *Manikyamba* et al., 2004). If this is the case, the mechanism of infiltration of high Ni, Co, Cr komatiitic liquids into the mantle wedge under intra-oceanic arc prior to arc magmatism (*Parman* et al., 2003), could be used to explain why the studied rocks have greater concentrations of Ni and Cr, in comparison with modern basalts from various settings (e.g. MORBs and island arc basalts). Conclusively, the magma for the studied rocks did not originate from asthenospheric melts that stand for N-MORB composition, but from a plume-influenced mantle wedge in an intra-oceanic arc/suprasubduction zone tectonic setting.

Petrogenesis

In the Ti/Cr *vs.* Ni discrimination diagram (Fig. 15), the studied rocks plot in the same field as the Late Cretaceous ophiolite from Baer-Bassit area, implying a transition from MORB-like, ocean island arc basalts to boninite-like rocks (e.g. *Al-Riyami* et al., 2002). Typically, such an evolution is commonly related to the early stage island-arc formation (proto-forearc), and generally reflects progressive melting of a mantle source becoming increasingly depleted (*Saccani* and *Photiades*, 2004). The Group 1 samples appear to show back-arc tholeiite affinity (BABB-type) and compositionally are comparable to basaltic rocks from the Lau back-arc basin (*Ewart* et al., 1998). However, their low Ti/V ratios (<20) are

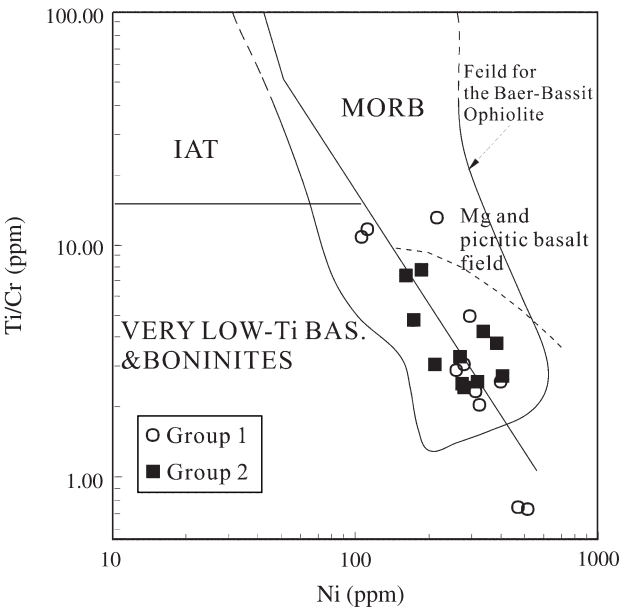

Fig. 15. Plots of Ni vs. Ti/Cr for the Tunchang area metabasites (after *Beccaluva* and *Serri*, 1988). The Baer-Bassit Ophiolite from *Al-Riyami* et al. (2002); some data for the Group 2 are from *Li* et al. (2002)

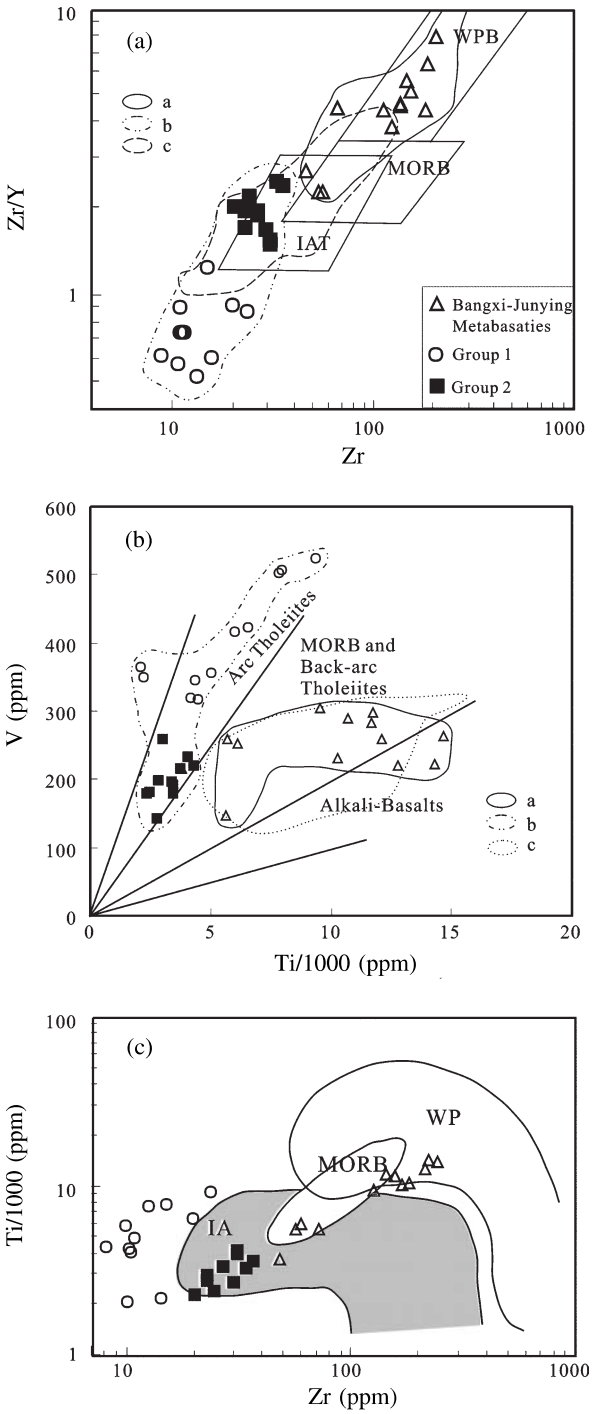

Fig. 16. Plots of Zr vs. Zr/Y (**a**), V vs. Ti/1000 (**b**) and Zr vs. Ti/1000 (**c**) for metabasites both from the Tunchang and the Bangxi areas, after *Pearce* and *Norry* (1979), *Shervais* (1982) and *Woodhead* et al. (1993). *WPB* Within Plate Basalts, *MORB* Mid Ocean Ridge Basalts, *IAT* Island Arc Basalts. Field (a) for the Bangxi area metabasites from *Xia* et al. (1991), *Fang* et al. (1992), *Xu* et al. (2001) and *Li* et al. (2002), field (b) for the Tunchang area metabasites from *Li* et al. (2002) and this study, field (c) in (**a**) from *Al-Riyami* et al. (2002) and field (c) in **b** from *Zhang* et al. (1994)

consistent with arc tholeiites rather than back-arc basalts (Fig. 16), marking an immature intra-oceanic arc rather than a mature (rifted) volcanic arc (*Wang* et al., 2002). The ratio of Zr/Nb (6–73) also suggests that the studied rocks are not derived from back-arc mantle source, which is characterized by Zr/Nb ratio close to that for MORB, but from a primitive arc source (Zr/Nb = 9–87: *Pearce* and *Peate*, 1995).

We thus conclude that the studied rocks were produced during the initiation of a primitive island arc and are associated with the initiation of subduction.

The emergence of the IAT and boninitic-like rocks in the studied area indicates a combined result of a dispersed volatile component, decompressional melting of mantle at fairly low pressures (fore-arc extension) and a depleted mantle source, during the subduction of juvenile oceanic crust beneath a young, hot overriding plate (e.g. *Taylor* et al., 1994). Hence, the source for the Tunchang metabasites appears to have had at least three stages of petrogenetic history. Before the initiation of subduction of a young ocean lithosphere, the depleted oceanic mantle wedge after extraction of melts might have been infiltrated by a high Ni, Co, Cr komatiitic liquid due to the activity of a pre-existing mantle plume (*see the discussion above*). This stage probably had produced high concentrations of Cr and Ni, and led the depleted mantle wedge source to be highly heterogenous. During the initiation of subduction, partial melting of the depleted oceanic mantle wedge as induced by release of metasomatic agents from the subducted oceanic lithosphere would generate parental melts to the protolith for the studied rocks. The variable degrees of partial melting, however, might have resulted in two primitive arc magma types at different depth levels, which are responsible for formation of the Group 1 and the Group 2 rocks, respectively. When these two magma types rise and move to the fore-arc regime during a slightly late stage, fractional crystallization of clinopyroxene $\pm$ olivine $\pm$ plagioclase might have occurred, which eventually led to formation of the prolioths for the Tunchang area metabasites.

Tectonic implications

Previous studies (*Xia* et al., 1991; *Fang* et al., 1992) regarded the metabasites within the Paleozoic volcanic-clastic sedimentary sequences in Hainan Island, South China as of Late Paleozoic age, owing to the presence of Carboniferous-Permian fossil fragments in the associated sedimentary rocks. *Li* et al. (2002) also obtained a Sm-Nd whole rock isochron age of $\sim$330 Ma for metabasites both in the Tunchang area (East-central Island) and the Bangxi area (northwestern part of Hainan Island: Fig. 1). They further suggested that the metabasites the two sites were derived from a similar mantle source and represent remnants of the Paleo-Tethys; accordingly, they were named ''Bangxi-Chenxing ophiolite''. However, the present study reveals that the metabasites in the Tunchang area are distinct in bulk rock geochemistry and Sr-Nd isotopes from the metabasites in the Bangxi area. Compositionally, the Bangxi area metabasites show low but variable SiO_2 contents (40.7–54.3 wt.%), high but variable TiO_2 (up to 2.5 wt.%) and Na_2O (up to 3.5 wt.%) contents, and high but variable Zr (50–250 ppm), Y (12.50–43.50 ppm), Cr (285–1348 ppm) and Ni (48–1219 ppm) concentrations (c.f. *Xia* et al., 1991; *Fang* et al., 1992; *Xu* et al., 2001; *Li* et al., 2002). These rocks also have high but variable REE concentrations (24–120 ppm) and generally occupy LREE-enriched distribution patterns with minor occurrence of LREE-depleted type. The ε_{Nd} (330 Ma) values (-3.17 to $+7.80$) (*Fang* et al., 1992; *Li* et al., 2002) reflect a highly depleted to enriched mantle source. Thus the protoliths for the Bangxi area metabasites most likely were formed during extension in a back-arc basin or a marginal basin due to the activity of a mantle plume (e.g. *Jahn*, 1986).

The extension of the basin probably was quick so that a small oceanic basin could have been generated at that time, as can be inferred from the geochemical signature (e.g. the occurrence of N-MORB-like compositions, *Fang* et al., 1992; *Li* et al., 2002) and the geological observation (e.g. an extrusive feature of submarine facies for these rocks, *Xia* et al., 1991).

Preliminary SHRIMP II U-Pb zircon dating also shows a minimum age of 450 Ma for the protoliths of the Tunchang area metabasites whereas an age of 270 Ma for those in the Bangxi area (*Xu* et al., 2007). Thus, magmatism both in the Tunchang and the Bangxi areas more likely represents two different tectono-magmatic events. Indeed, the Bangxi area metabasites are more comparable to the Shuanggou ophiolites in the Honghe-Ailaoshan suture zone (Figs. 1a and 16b), owing to the closure of the Paleo-Tethys between the South China and the Indosinian Blocks. Moreover, *Zhang* et al. (1994) suggested a small oceanic basin, likely responding to slow-spreading ridge, responsible for the generation of the Shuanggou ophiolites. The Paleozoic island arc-type basaltic rocks in the Chenxi area, Guangxi Province, South China, which formed due to the subduction of the Paleo-Tethys under the South China continental margin, have an extrusive age of 261 Ma (*Zhang* et al., 1997). On Hainan Island, the typical calc-alkaline I-type granites formed in an active continental margin in the Qiongzhong area also have a SHRIMP zircon U-Pb age of 267–262 Ma (*Li* et al., 2006). We thus suggest that the subduction of the Paleo-Tethys beneath the South China continental margin probably led to the opening of a back-arc basin and subsequent formation of a small oceanic basin where the protoliths of the Bangxi area metabasites were formed. The widespread Hercynian-Indosinian syncollisional S-type granites (240 Ma , SHRIMP zircon U-Pb age, *Li* et al., 2005) more likely mark the late Permain-earliest Triassic collision due to the closure of the Paleo-Tethys along the Changjiang-Qionghai fault zone on Hainan Island (Fig. 1b).

Trilobite faunal occurrences and paleomagnetic data suggest that Hainan Island when Gondwana was formed in the Early Cambrian likely was part of the northern extension of the continental ribbon including Tasmania and South China Block adjacent to the eastern Australia mainland (*Li* and *Powell*, 2001). If this was the case, the westward subduction of the Paleo-Pacific plate along the eastern margin of Australia-Antarctica during the Cambrian (see Fig. 7 in *Li* and *Powell*, 2001) probably led to formation of an Early Paleozoic intraoceanic arc adjacent to the active continental margin of South China Block. This suggestion can be supported by that the metavolcanic rocks with continental arc signatures, which occur as interlayers within the early Paleozoic felsic schists in the studied area, have a zircon U-Pb age of 528 ± 48 Ma (*Ding* et al., 2002). If the metabasites in the Qionghai and southern Ledong regions, southeast Hainan Island (Fig. 1b), show the same geochemical components and ages as those in the Tunchang area, then the NE-SW-trending Baisha Fault Zone (Fig. 1b) most likely marks the location of the earliest suture due to the collision of the Early Paleozoic intraoceanic island arc with the active continental margin of South China Block. This event probably is recorded in the Pre-Carboniferous rocks in South China which were strongly deformed, and in the underlying early Paleozoic rocks, which generally have a high-angular unconformity with the overlying Carboniferous rocks (*Zhang* et al., 1997). Nevertheless, more precise dating of the Paleozoic metabasites in Hainan Island is still needed.

Acknowledgements

This research was financially co-sponsored by Chinese Academy of Sciences (Grant No. KZCX2-YW-203) and China Natural Science Foundation (Grant No. 40473017). We would like to thank Yanhua Zhang (CSIRO, Australia) for his help in the revision of the manuscript. We are also grateful to Editor J. Raith, J. Foden and another anonymous reviewer for their careful reviews and constructive comments on the manuscript.

References

Al-Riyami K, Robertson A, Dixon J, Xenophontos C (2002) Origin and emplacement of the Late Cretaceous Baer-Bassit ophiolite and its metamorphic sole in NW Syria. Lithos 65: 225–260

Arndt NT, Nisbet EG (1982) Komatiites. George Allen & Unwin Ltd, London, UK, pp 1–383

Beccaluva L, Serri G (1988) Boninitic and low-Ti subduction-related lavas from intraoceanic arc-backarc systems and low-Ti ophiolites: a reappraisal of their petrogenesis and original tectonic setting. Tectonophysics 146: 291–315

Bédard JH (1999) Petrogenesis of boninites from the Betts Cove ophiolite, Newfoundland, Canada: identification of subducted source components. J Petrol 40: 1853–1889

Benoit M, Polvé M, Ceuleneer G (1996) Trace element isotopic characterization of mafic cumulates in a fossil mantle diapir (Oman ophiolite). Chem Geol 134: 199–214

Brewer TS, Menuge JF (1998) Metamorphic overprinting of Sm-Nd isotopic systems in volcanic rocks: the Telemark Supergroup, southern Norway. Chem Geol 145: 1–16

Constantin M (1999) Gabbroic intrusions and magmatic metasomatism in harzburgites from the Garrett transform fault: implications for the nature of the mantle-crust transition at fast-spreading ridges. Contrib Mineral Petrol 136: 111–130

Coogan LA, Banks GJ, Gillis KM, MacLeod CJ, Pearce JA (2003) Hidden melting signatures recorded in the Troodos ophiolite plutonic suite: evidence for widespread generation of depleted melts and intra-crustal melt aggregation. Contrib Mineral Petrol 144: 484–505

Coogan LA, MacLeod CJ, Dick HJB, Edwards SB, Kvassnes A, Natland JH, Robinson PT, Thompson G, O'Hara MJ (2001) Whole-rock geochemistry of gabbros from the Southwest Indian Ridge: constraints on geochemical fractionations between the upper and lower oceanic crust and magma chamber processes at very slow-spreading ridges. Chem Geol 178: 1–22

Cullers RL, Graf JL (1984) Rare earth elements in igneous rocks of the continental crust: predominantly basic and ultrabasic rocks. In: *Henderson P* (ed) Rare earth element geochemistry. Elsevier, Amsterdam, pp 237–274

Ding Sh-J, Xu Ch-H, Long W-G, Zhou Z-Y, Liao Z-T (2002) Tectonic attribute and geochronology of meta-volcanic rocks, Tunchang, Hainan Island. Acta Petrologica Sinica 18: 83–90 (in Chinese with English abstract)

Erlank AJ, Duncan AR, Marsh JS, Sweeney RJ, Hawkesworth CJ, Milner SC, Miller RMcG, Rogers NW (1988) A laterally extensive geochemical discontinuity in the subcontinental Gondwana Lithosphere. In: Geochemical Evolution of the Continental Crust, Conf Abstr Procos de Caldes, Brazil, 11–16 July 1988, pp 1–10

Ewart A, Collerson KD, Regelous M, Wendt JI, Niu Y (1998) Geochemical evolution within the Tonga-Kermadec-Lau arc-back-arc systems: the role of varying mantle wedge composition in space and time. J Petrol 39: 331–368

Fang Z, Zhao JX, McCulloch MT (1992) Geochemical and Nd isotopic study of Paleozoic bimodal volcanics in Hainan Island, South China – implications of rifting tectonics and mantle reservoirs. Lithos 29: 127–139

Faure G (2001) Origin of igneous rocks: the isotopic evidence. Springer-Verlag, Berlin Heidelberg New York, Germany, pp 103–156

Gill JB (1981) Orogenic andesites and plate tectonics. Springer-Verlag, Berlin Heidelberg New York, pp 1–390

Halkoaho T, Liimatainen J, Papunen H, VaÈlimaa J (2000) Exceptionally Cr-rich basalts in the komatiitic volcanic association of the Archaean Kuhmo greenstone belt, eastern Finland. Mineral Petrol 70: 105–120

Harry DL, Green NL (1999) Slab dehydration and basalt petrogenesis in subduction systems involving very young oceanic lithosphere. Chem Geol 160: 309–333

Hart SR, Staudigel H (1982) The control of alkalies and uranium in sea water by ocean crust alteration. Earth Planet Sci Lett 58: 202–212

Hawkesworth CJ, Gallagher K, Hergt JM, McDermott F (1993) Mantle and slab contributions in arc magmas. Ann Rev Earth Planet Sci Lett 21: 175–204

Hoernle KAJ (1998) Geochemistry of Jurassic oceanic crust beneath Gran Canaria (Canary Islands): implications for crustal recycling and assimilation. J Petrol 39: 859–880

Hofmann AW (1988) Chemical differentiation of the Earth. The relationship between mantle, continental crust and oceanic crust. Earth Planet Sci Lett 90: 297–314

Hole MJ, Saunders AD, Marriner GF, Tarney J (1984) Subduction of pelagic sediments: implications for the origin of Ce-anomalous basalts from the Mariana Islands. J Geol Soc London 141: 453–472

Hollings P, Kerrich R (2004) Geochemical systematics of tholeiites from the 2.86 Ga Pickle Crow assemblage, northwestern Ontario: arc basalts with positive and negative Nb-Hf anomalies. Precamb Res 134: 1–20

Jahn B (1986) Mid-ocean ridge or marginal basin origin of the East Taiwan ophiolite: chemical and isotopic evidence. Contrib Mineral Petrol 92: 194–206

Kelemen PB, Koga K, Shimizu N (1997) Geochemistry of gabbro sills in the crust-mantle transition zone of the Oman ophiolite: implications for the origin of the oceanic lower crust. Earth Planet Sci Lett 146: 475–488

La Fléche MR, Camire G, Jenner GA (1998) Geochemistry of post-Acadian, Carboniferous continental intraplate basalts from the Maritimes Basin, Magdalen Islands, Que'bec, Canada. Chem Geol 148: 115–136

Leybourne MI, Van Wageoner NA, Ayres LD (1997) Chemical stratigraphy and petrogenesis of the Early Proterozoic Amisk Lake volcanic sequence, Flin Flon-Snow Lake greenstone belt, Canada. J Petrol 38: 1541–1564

Li SX, Yun P, Fan Y, Zhou JP (2005) Zircon U-Pb age and its geological significance for Qiongzhong pluton in Qiongzhong area, Hainan Island. Geotectonica et Metallogenia 29: 234–241 (in Chinese with English abstract)

Li XH, Li ZX, Li WX, Wang YJ (2006) Initiation of the Indosinian Orogeny in South China: Evidence for a Permian magmatic arc on Hainan Island. J Geol 114: 341–353

Li XH, Zhou HW, Chung SL, Ding SJ, Liu Y, Lee CY, Ge WC, Zhang YM, Zhang RJ (2002) Geochemical and Sm-Nd isotopic characteristics of metabasites from central Hainan Island, South China and their tectonic significance. Island Arc 11: 193–205

Li ZX, Li XH, Kinny PD, Wang J (1999) The breakup of Rodinia: Did it start with a mantle plume beneath South China? Earth Planet Sci Lett 173: 171–181

Li ZX, Powell CMcA (2001) An outline of the palaeogeographic evolution of the Australasian region since the beginning of the Neoproterozoic. Earth Sci Rev 53: 237–277

Lu M-H, Hofmann AW, Mazzucchelli M, Rivalenti G (1997) The mafic-ultramafic complex near Finero (Ivrea-Verbano zone), II. Geochronology and isotope geochemistry. Chem Geol 140: 223–235

Ma CQ, Li ZC, Ehlers C, Yang KG, Wang RJ (1998) A post-collisional magmatic plumbing system: Mesozoic granitoid plutons from the Dabieshan high-pressure and ultrahigh-pressure metamorphic zone, east-central China. Lithos 45: 431–456

Magganas AC (1990) Relict minerals of metavolcanic and meta-pyroclastic rocks from the Circum-Rhodope Belt in the area of Thrace, Greece. Geologica Rhodopica 2: 251–262

Manikyamba C, Kerrich R, Naqvi SM, Mohan MR (2004) Geochemical systematics of tholeiitic basalts from the 2.7 Ga Ramagiri-Hungund composite greenstone belt, Dharwar craton. Precamb Res 134: 21–39

Metcalfe I, Shergold IH, Li ZX (1993) IGCP 321 Gondwana dispersion and Asian accretion: fieldwork on Hainan island. Episodes 16: 443–447

Parman SW, Shimizu N, Grove1 TL, Dann JC (2003) Constraints on the pre-metamorphic trace element composition of Barberton komatiites from ion probe analyses of preserved clinopyroxene. Contrib Mineral Petrol 144: 383–396

Pearce JA (1983) Role of the sub-continental lithosphere in magma genesis at active continental margins. In: *Hawkesworth CJ, Norry MJ* (eds) Continental flood basalts and mantle xenoliths. Shiva, Nantwich, UK, pp 230–249

Pearce JA, Norry MJ (1979) Petrogenetic implications of Ti, Zr, Y and Nb variations in volcanic rocks. Contrib Mineral Petrol 69: 33–47

Pearce JA, Peate DW (1995) Tectonic implications of the composition of volcanic arc magmas. Ann Rev Earth Planet Sci Lett 23: 251–285

Polat A, Hofmann AW, Rosing MT (2002) Boninite-like volcanic rocks in the 3.7–3.8 Ga Isua greenstone belt, West Greenland: geochemical evidence for intra-oceanic subduction zone processes in the early Earth. Chem Geol 184: 231–254

Robertson AHF (2002) Overview of the genesis and emplacement of Mesozoic ophiolites in the Eastern Mediterranean Tethyan region. Lithos 65: 1–67

Rolland Y, Picard C, Pecher A, Lapierre H, Bosch D, Keller F (2002) The Cretaceous Ladakh arc of NW Himalaya – slab melting and melt-mantle interaction during fast northward drift of Indian Plate. Chem Geol 182: 139–178

Rudnick RL, Fountain DM (1995) Nature and composition of the continental crust: a lower crustal perspective. Rev Geophys 33: 267–309

Saccani E, Photiades A (2004) Mid-ocean ridge and supra-subduction affinities in the Pindos ophiolites (Greece): implications for magma genesis in a forearc setting. Lithos 73: 229–253

Shervais JW (1982) Ti, V plot and the petrogenesis of modern and opholitic lavas. Earth Planet Sci Lett 59: 101–118

Staudigel H, Davies GR, Hart SR, Marchant KM, Smith BM (1995) Large scale isotopic Sr, Nd and O isotopic anatomy of altered oceanic crust: DSDP/ODP sites 417/418. Earth Planet Sci Lett 130: 169–185

Sun S-S, McDonugh WF (1989) Chemical and isotopic systematics of oceanic basalt: implication for mantle composition and processes. In: *Saunders AD, Norry MJ* (eds) Magmatism in the ocean basins. Geol Soc Spec Publ 42: 528–548

Tatsumi Y, Eggins S (1995) Subduction zone magmatism. Blackwell, London, pp 211

Taylor RN, Nesbitt RW, Vidal P, Harmon RS, Auvray B, Croudace IW (1994) Mineralogy, chemistry, and genesis of the boninite series volcanics, Chichijima, Bonin Islands, Japan. J Petrol 35: 577–617

Teklay M, Kröner A, Mezger K (2002) Enrichment from plume interaction in the generation of Neoproterozoic arc rocks in northern Erit area: implications for crustal accretion in the southern Arabian-Nubian Shield. Chem Geol 184: 167–184

Wang Z-H, Shu S, Li J-L, Hou Q-L (2002) Petrogenesis of tholeiite associations in Kudi ophiolite (western Kunlun Mountains, northwestern China): implications for the evolution of back-arc basins. Contrib Mineral Petrol 143: 471–483

Winchester JA, Floyd PA (1977) Geochemical discrimination of different magma series and their differentiation products using immobile elements. Chem Geol 20: 325–343

Woodhead J, Eggins S, Gamble J (1993) High field strength and transition element systematics in island arc and back-arc basin basalts: evidence for multi-phase melt extraction and a depleted mantle wedge. Earth Planet Sci Lett 114: 491–504

Xia BD, Yu JH, Fang Z, Wang CY, Shi GY (1991) The Carboniferous bimodal volcanic rocks in Hainan Island and their plate tectonic setting. Acta Petrologica Sinica 7: 54–62 (in Chinese with English abstract)

Xu DR, Lin G, Liang XQ, Chen GH, Tang HF (2001) The records of the evolution of Precambrian lithosphere – the evidences of petrology and geochemistry of basic rocks on Hainan Island. Acta Petrologica Sinica 17: 589–609 (in Chinese with English abstract)

Xu DR, Xia B, Li PC, Chen GH, Zhang YQ, Ma C (2007) Protolith natures and U-Pb SHRIMP zircon ages of the metabasites in Hainan Island, South China: implications for geodynamic evolution since the late Precambrian. The Island Arc (in press)

Xu DR, Xia B, Nonna BC, Ma C, Li PC, Robert B, Chen GH (2006) Metamorphic characteristics of the Chenxing metabasite massif in Tunchang area, Hainan Island, South China and its tectonic implication. Acta Petrologica Sinica 22: 3987–3006 (in Chinese with English abstract)

Yibas B, Reimold WU, Anhaeusser CR, Koeberl C (2003) Geochemistry of the mafic rocks of the ophiolitic fold and thrust belts of southern Ethiopia: constraints on the tectonic regime during the Neoproterozoic (900–700 Ma). Precamb Res 121: 157–183

Yumul GP Jr (2003) The Cretaceous southeast Bohol ophiolite complex, Central Philippines: a highly disaggregated supra-subduction zone ophiolite. J Asian Earth Sci 21: 957–965

Zhang BY, Zhao ZH, Shi MQ, Yang SF, Chen HL (1997) The confirmation of the Permian island arc basalt in Chenxi area and its tectonic significance: implication for Paleo-Tethys tectonic zone in the boundary between Guangdong and Guangxi Provinces. Chinese Sci Bulletin 42: 413–416

Zhang Q, Zhou DJ, Zhao DS, Huang ZX, Han S, Jia AQ, Dong JQ (1994) Ophiolites of the Hengduan Mountains, China: Characteristics and tectonic settings. J Southeast Asian Earth Sci 9: 335–344

Zhang YM, Xu AW, Fu JM, Zhao ZJ, Wu GJ, Zeng BF (1997) Some important fundamental geological problems in Hainan Island. Geological Review 44: 568–575 (in Chinese with English abstract)

Zimmer M, Kröner A, Jochum KP, Reischmann T, Todt W (1995) The Gabal Gerf complex: a Precambrian N-MORB ophiolite in the Nubian shield, NE Africa. Chem Geol 123: 29–51

Zindler A, Jagoutz E, Goldstein S (1982) Nd-Sr and Pb isotopic systematics in a three-component mantle: a new perspective. Nature 298: 519–523

Authors' addresses: *Deru Xu* (e-mail: xuderu@gig.ac.cn), *Bin xia* (e-mail: xiabin@gig.ac.cn), *Pengchun Li* (e-mail: li788@gig.ac.cn), *Guanghao Chen* (e-mail: chengh@gig.ac.cn), *Tao Chen* (e-mail: chengtao@gig.ac.cn), Key Lab of Marginal Sea Geology, Chinese Academy of Sciences, Guangzhou Institute of Geochemistry, Guangzhou, Guangdong Province 510640, People's Republic of China; *Bakun-Czubarow Nonna* (e-mail: nbakun@twarda.pan.pl), *Bachlinski Robert* (e-mail: robach@twarda.pan.pl), Polish Academy of Sciences, Institute of Geological Sciences, Institute of Geological Sciences, ul. Twarda 51/55, 00-818 Warszawa, Poland